The *Chlamydomonas* Cell Wall and Its Constituent Glycoproteins Analyzed by the Quick-Freeze, Deep-Etch Technique

URSULA W. GOODENOUGH and JOHN E. HEUSER
Departments of Biology and Cell Biology/Biophysics, Washington University, St. Louis, Missouri 63130

ABSTRACT Using the quick-freeze, deep-etch technique, we have analyzed the structure of the intact cell wall of *Chlamydomonas reinhardi*, and have visualized its component glycoproteins after mechanical shearing and after depolymerization induced by perchlorate or by the wall-disrupting agent, autolysin. The intact wall has previously been shown in a thin-section study (Roberts, K., M. Gurney-Smith, and G. J. Hills, 1972, *J. Ultrastruct. Res.* 40:599–613) to consist of a discrete central triplet bisecting a meshwork of fibrils. The deep-etch technique provides additional information about the architecture of each of these layers under several different experimental conditions, and demonstrates that each layer is constructed from a distinct set of components. The innermost layer of the central triplet proves to be a fibrous network which is stable to perchlorate but destabilized by autolysin, disassembling into fibrillar units we designate as "fishbones." The medial layer of the triplet is a loose assemblage of large granules. The outer layer is a thin, crystalline assembly that is relatively unaffected by autolysin. It depolymerizes into two glycoprotein species, one fibrous and one globular. The wall glycoproteins prove to be structurally similar to two fibrous proteins that associate with the flagellar membrane, namely, the sexual agglutinins and the protomers of a structure we designate a "hammock." They are also homologous to some of the fibrous components found in the extracellular matrices of multicellular plants and animals. The quick-freeze, deep-etch technique is demonstrated to be a highly informative way to dissect the structure of a fibrous matrix and visualize its component macromolecules.

It is becoming increasingly clear that interactions between cells often involve the molecular merger of their extracellular matrices and/or the establishment of a common extracellular matrix. During the formation of a bilayered epithelium in animals, for example, an essential event is the formation of a common basal lamina, rich in such fibrous glycoproteins as type IV collagens and laminin (for review see reference 1), which is produced and secreted by both types of epithelial cells. In the case of higher plants, the initial event in cell wall formation appears to be the secretion of a fibrous hydroxyproline-rich glycoprotein, named extensin, accompanied by the deposition of such polysaccharides as pectins and cellulose (for review see reference 2).

The unicellular alga *Chlamydomonas reinhardi* is surrounded by an extracellular coat composed of hydroxyproline-rich glycoproteins (3–5). An extracellular matrix of similar material holds together the individual *Chlamydomonas*-type cells that form such colonial genera as *Pandorina* and *Volvox* (6–8). It is therefore reasonable to imagine that there may be evolutionary relationships between the matrix of *Chlamydomonas* and of the true metazoa. This article presents an analysis of how this matrix is constructed, using the quick-freeze, deep-etch technique developed in one of our laboratories (9, 10).

The central region of the *Chlamydomonas* wall has previously been shown to be trilaminar and highly ordered (11–16), analogous to the layered construction of the glomerular basal lamina (17). Here we demonstrate that each of the ordered layers contains a characteristic population of distinct glycoproteins. Deep-etch visualization of the molecules obtained by several different extraction protocols demonstrates that some wall components are fibrous and others are globular. Partial dissolution and/or reconstitution experiments, coupled with deep-etching, demonstrate several specific interactions between these components. Since several of the spatial arrays on the cell surface are very regular and two-dimen-

THE JOURNAL OF CELL BIOLOGY · VOLUME 101 October 1985 1550–1568

sional, it should be possible to analyze the rules followed during their construction. Some of these rules may prove to be followed during assembly of the more complex, three-dimensional arrays that usually characterize the extracellular matrices of higher eukaryotes.

MATERIALS AND METHODS

Strains and Culture Conditions: The wild-type strains CC-620 (mt^+) and CC-621 (mt^-) were both derived from strain 137c (all CC numbers refer to stocks available from the *Chlamydomonas* Genetics Center, Department of Botany, Duke University, Durham, NC 27706). We also examined wall material from the Norwich wild-type strain kindly provided by Dr. Keith Roberts, John Innes Institute, Norwich, England, and found it to have an identical structure to our wild-type strain. In certain experiments we used *bald-2* (CC-478), a basal body–defective mutant (18) which accumulates several layers of cell walls during vegetative growth and lacks the flagella which would otherwise contaminate whole cell extracts. Gametes were harvested from Tris-acetate-phosphate (19) plates after 7 d of growth as described (20) and suspended in nitrogen-free high salt medium (21); vegetative cells were grown in constant light in liquid TAP medium for 36–48 h. The Norwich strain was grown in liquid yeast/acetate/peptone medium (22) for 5 d.

Isolation and Mechanical Breakage of Cell Walls: Walls were isolated from vegetative *bald-2* cells as previously described (16) except that detergent was not used; the walls were washed free of sucrose and suspended in 10 mM HEPES, pH 7.4, 5 mM $MgSO_4$, 100 mM KCl after purification.

Walls were isolated from wild-type gametes by mixing 10^{10} cells of each mating type together at a final cell density of 5×10^7 and allowing them to agglutinate until, by phase-contrast microscopy, the field was filled with walls released by the action of autolysin (usually 1–2 min). EDTA concentrate (1 M) was then added to a final concentration of 12 mM, in order to quench the activity of autolysin (23). The walls were harvested and purified by centrifugation, taking advantage of the fact that the walls form a loose fluffy layer above any material that pellets at 40,000 *g* (14); therefore, if most of the supernatant above this layer is carefully pipetted off and the centrifuge tube is gently tapped, the walls become suspended in the residual supernatant and can be pipetted away from the underlying pellet. The fraction is then diluted with fresh 12 mM EDTA/HEPES and the procedure is repeated until no solid pellet forms when the preparation is centrifuged. By phase-contrast microscopy, this material consists of egg-shaped walls torn only at their anterior ends (24), plus large wall segments.

Walls isolated from *bald-2* or gametic cells were suspended in 30 mM HEPES, pH 7.4, 100 mM KCl, 5 mM $MgSO_4$, and 0.5 mM EDTA (HKMgE), and disrupted either by ultrasonic disintegration using a Fisher device with a microprobe operating at 70 W for two 30-s intervals, or by shearing in a Virtis homogenizer operating at top speed for 1–2 min. The samples were then pelleted at 40,000 *g* for 10 min. Both the pelleted and the supernatant material was mixed with freshly cleaved mica flakes and quick-frozen (10); similar results were obtained with both fractions.

Perchlorate Solubilization and Fractionation of Walls: Isolated gametic walls were mixed with an equal volume of 2 M perchlorate in distilled water. Phase-contrast microscopy demonstrated that the initially phase-dense walls were converted to barely detectable "inner walls" (14) after 15 min. The inner walls were pelleted by centrifugation at 100,000 *g* for 30 min. In some experiments the supernatant was loaded on a Sepharose 2B column as described by Catt et al. (5) and eluted with 1 M perchlorate, collecting 2-ml fractions. Each fraction was dialyzed against several changes of distilled water over a 2-d period. Aliquots of each were then lyophilized, solubilized in SDS/urea/dithiothreitol, and analyzed by SDS PAGE using a 4–15% slab gel system as previously described (16). Fractions with polypeptide compositions comparable to the 2BII fractions of Catt et al. (5) were examined and found to contain small phase-dense aggregates. These were pelleted, suspended in a small volume of HKMgE (the salt being necessary for adsorption to mica), mixed with mica flakes, and quick-frozen (10). Inner walls were washed in water and frozen in HKMgE; in some cases they were boiled for 3 min in lysis buffer containing 400 mM dithiothreitol before electrophoresis.

Perchlorate extracts were also prepared by suspending living *bald-2* vegetative cells harvested from a 5-liter liquid Tris-acetate-phosphate culture in 1 M perchlorate for 20 min with gentle agitation. The cells remain physically intact (no chlorophyll contaminates the supernatant) but are killed by the treatment (no growth occurs when they are plated out). The supernatant is dialyzed against 12 liters of water (three changes), lyophilized, resuspended in 10 ml of 1 M perchlorate, and any insoluble material pelleted at 40,000 *g* for 10 min. The supernatant is dialyzed overnight against 4 liters of water to yield an abundance of large white crystals.

Mating Supernatants and Autolysin Preparation: Gametes of opposite mating type were mixed in nitrogen-free medium (21) at 10^7 cells/ml. After ~10 min of mating, the cells were pelleted at 2,000 *g* and the supernatant, containing depolymerizing walls, was allowed to stand at room temperature for 1 h, at which time no walls could be detected by phase-contrast microscopy. The supernatant was then spun at 40,000 *g* for 20 min to remove any particulate material, diluted fivefold with a salt solution containing 100 mM KCl, 5 mM $MgSO^4$, 10 mM HEPES, pH 7.4, and mixed with mica flakes for quick-freezing (10). Such supernatants were used as autolysin sources for the experiments illustrated in Figs. 12–14. For experiments investigating the effects of autolysin on purified "inner walls," the supernatants were spun at 100,000 *g* for 1 h to pellet all previously solubilized wall components, thereby permitting identification of the components released from the "inner walls."

Electron Microscopy: Both intact, unfixed cells and isolated cell walls were quick-frozen and deep-etched as described in references 9 and 10. Measurements were made using a Wild APT-1 stereo map reader interfaced with a Zeiss MOP-3 digitizing tablet and computer.

RESULTS

The Cell Wall In Situ

In a previous thin-section study, Roberts et al. (11) concluded that the cell wall of *C. reinhardi* is constructed of seven distinct layers; a diagram of their model is reproduced as Fig. 1*A*. When the wall is quick-frozen and cross-fractured, it is also possible to discern seven layers (Fig. 2). However, it

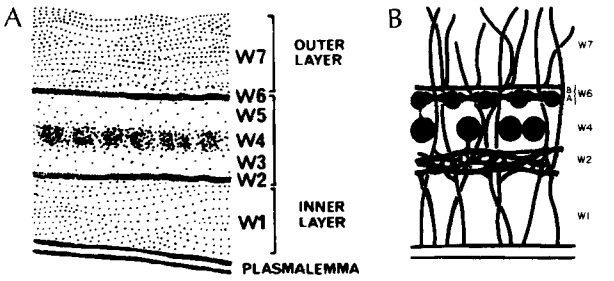

FIGURE 1 Diagram of the *C. reinhardi* cell wall based on the thin-section study (11) of Roberts et al. (*A*) and from the present study (*B*).

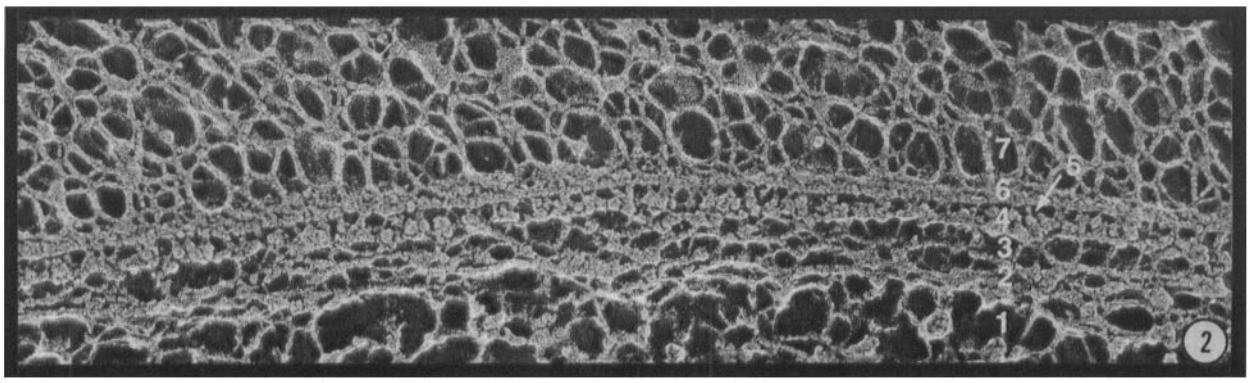

FIGURE 2 Cross-fractured intact cell wall. Layers 1–7 are labeled. × 130,000.

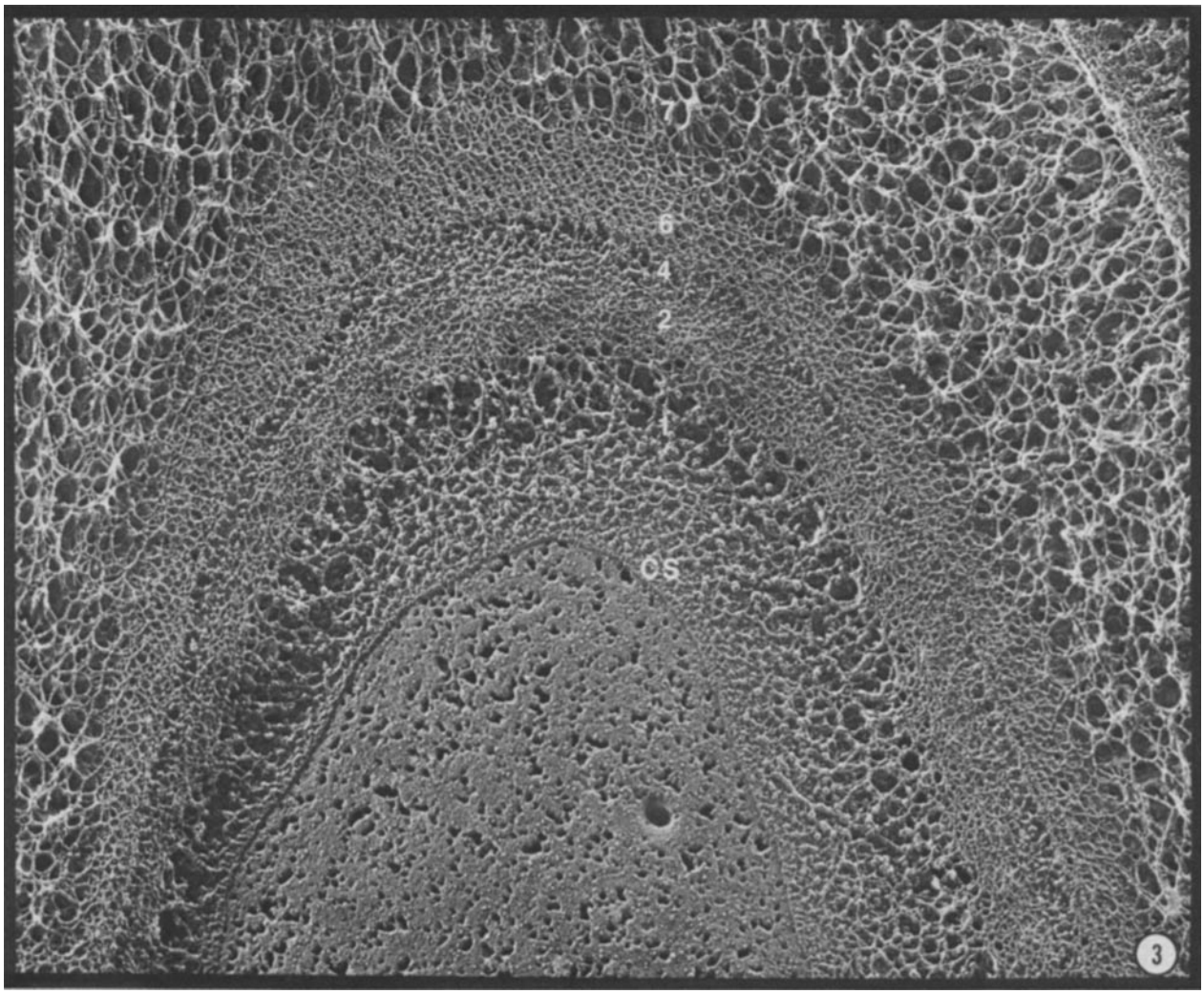

FIGURE 3 Wall in tangential fracure from intact cell. The cone-shaped central region is the P face of the plasma membrane, deeply pitted by the etching process. *CS* denotes the true cell surface. The major wall layers are numbered 1–7. × 65,000.

becomes clear that the domains designated W3 and W5 by Roberts et al. (Fig. 1*A*) are in fact spaces, transected by delicate strands, rather than true layers, a conclusion also reached by Dr. K. Roberts (personal communication). When the wall is fractured tangentially, which provides optimal views of the other layers, the W3 and W5 spaces are very difficult to identify. We therefore indicate the W3 and W5 regions when, as in Fig. 2, they can be identified, but in general refer to the wall as possessing five layers—W1, W2, W4, W6, and W7 (Fig. 1*B*)—retaining the Roberts numbering system to facilitate comparison between the two studies. We should note that Roberts has concluded that W2 and W6 are identical in substructure (15) whereas our studies indicate that they are distinctly different, a controversy that remains unresolved.

Fig. 3 shows a survey view of the cell and its wall in tangential fracture; Fig. 4 shows the "central triplet" (W2, W4, and W6) at higher magnification; and Figs. 5–11 show stereo views of the individual layers, all from quick-frozen, unfixed cells. In the paragraphs that follow we describe the architectural features of the wall that are revealed by these images, features summarized in the diagram presented as Fig. 1*B*.

W1 (FIG. 5): This region extends from the cell membrane to the inner dense layer of the triplet (cf. Fig. 3) and is quite variable in width from one cell to the next. Its constituent fibers, which vary in caliber, radiate outward from the membrane, making numerous side-to-side anastomoses with one another to create a three-dimensional trabeculum. A variable number of relatively large granules (Fig. 5, arrow), many 15–20 nm in diameter, associate with the fibers.

W2 (FIG. 6): This layer also appears to be a network of anastomosing fibers, but the "weave" is much tighter than the underlying W1 layer (cf. Figs. 3 and 5). Relatively thick fibers are interconnected by thinner fibers, the thick fibers tending to lie parallel to the cell surface (Fig. 2).

W4 (FIG. 7): The prominent components of this medial region of the wall are large granules, ~14 nm in diameter, which line up to form layer W4 as viewed in cross section (Figs. 1*A* and 2). Above and below the granules are thin strands, not visible in thin section (11), which occupy the electron-transparent layers denoted W3 and W5 by Roberts et al. (11) (see Fig. 1*A*); the W3 zone (3) is indicated in Fig. 6, and W5 (5) is shown in Fig. 7. When fractured *en face*, the W4 granules are found to be loosely aligned into chains that meander in a plane parallel to the cell surface. Often, these anastomosing chains appear to contain amorphous material between the granules, but this may simply represent confluence of adjacent granules.

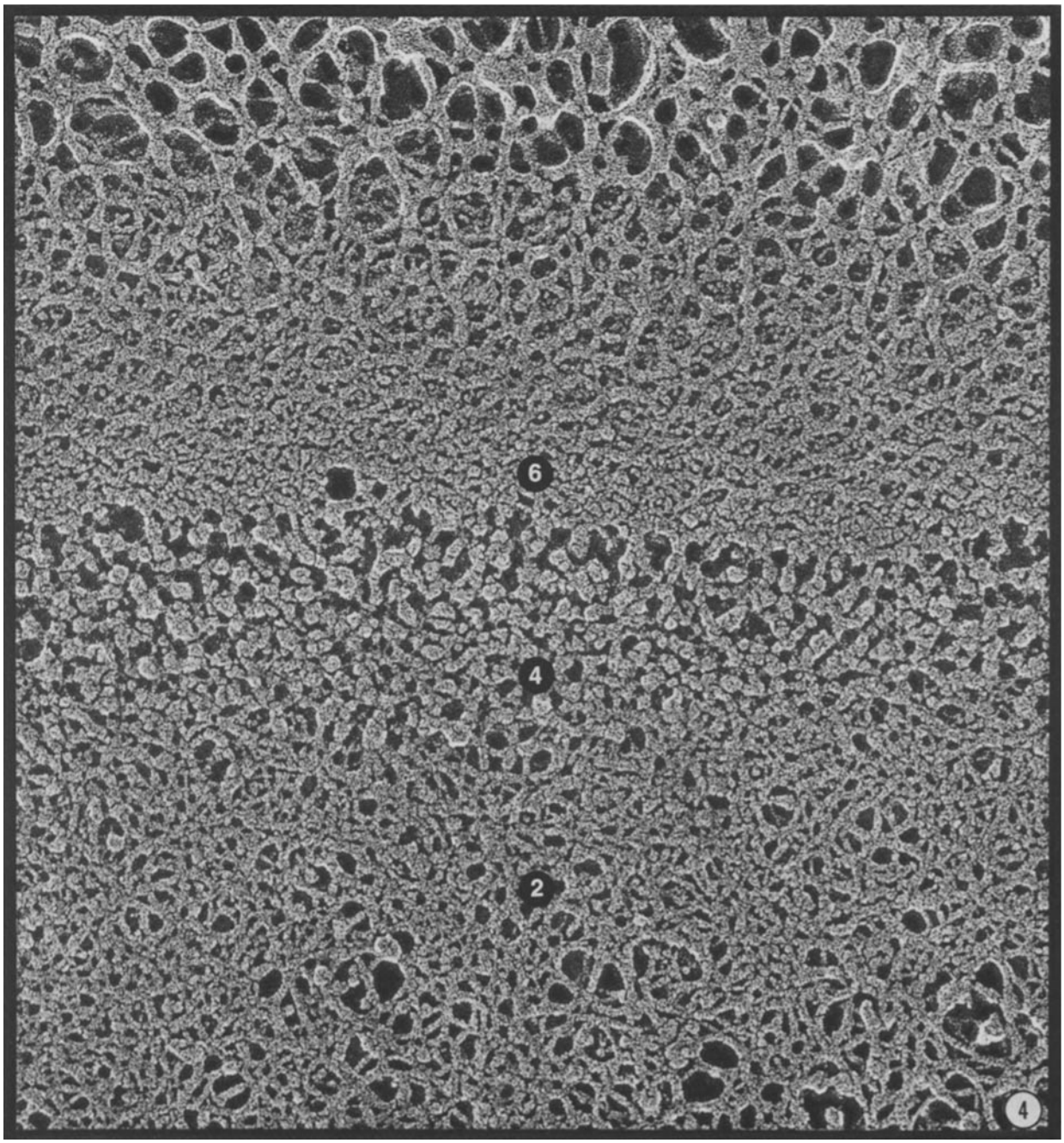

FIGURE 4 Central triplet (layers W2, W4, and W6) in tangential fracture from intact cell. × 215,000.

W6 (FIGS. 8 AND 9): This layer corresponds to the outer dense line of the central triplet (Fig. 1*A*). When fractured *en face* it proves to be composed of two discrete sublayers which we will designate W6A and W6B (Fig. 1*B*). W6A, which lies closer to the cell surface, is very densely woven, almost a mat (cf. Fig. 4), so that its construction can only be discerned when the weave has been pulled apart during fracturing, as in Fig. 8. The layer is then seen to be constructed from stout parallel fibers (running diagonally, 30° from the horizontal, from upper left to lower right in Fig. 8), which are interconnected by delicate cross-fibrils. The overlying sublayer W6B, by contrast, is an open weave (Figs. 6*B*, 8, and 9) which creates a polygonal lattice (see also Fig. 3). A and B are considered sublayers of W6 for reasons presented in a subsequent section.

W7 (FIGS. 10 AND 11): The constituent fibers of W7 are similar to those in W1: they radiate outward (Fig. 3) and make side-to-side anastomoses to form a trabeculum (Figs. 3 and 10). When adsorbed to mica flakes they retain this branching morphology (Fig. 11) and show no tendency to disassemble into subunits.

The Warp and Weft of the Cell Wall

When vegetative cells are stripped of their walls by the addition of exogenous autolysin, they re-grow new walls over a period of several hours (25). A detailed study of wall regeneration is in progress; here we show images of this process that are relevant to an understanding of wall construction. Immediately after autolysin treatment, the cell membrane is

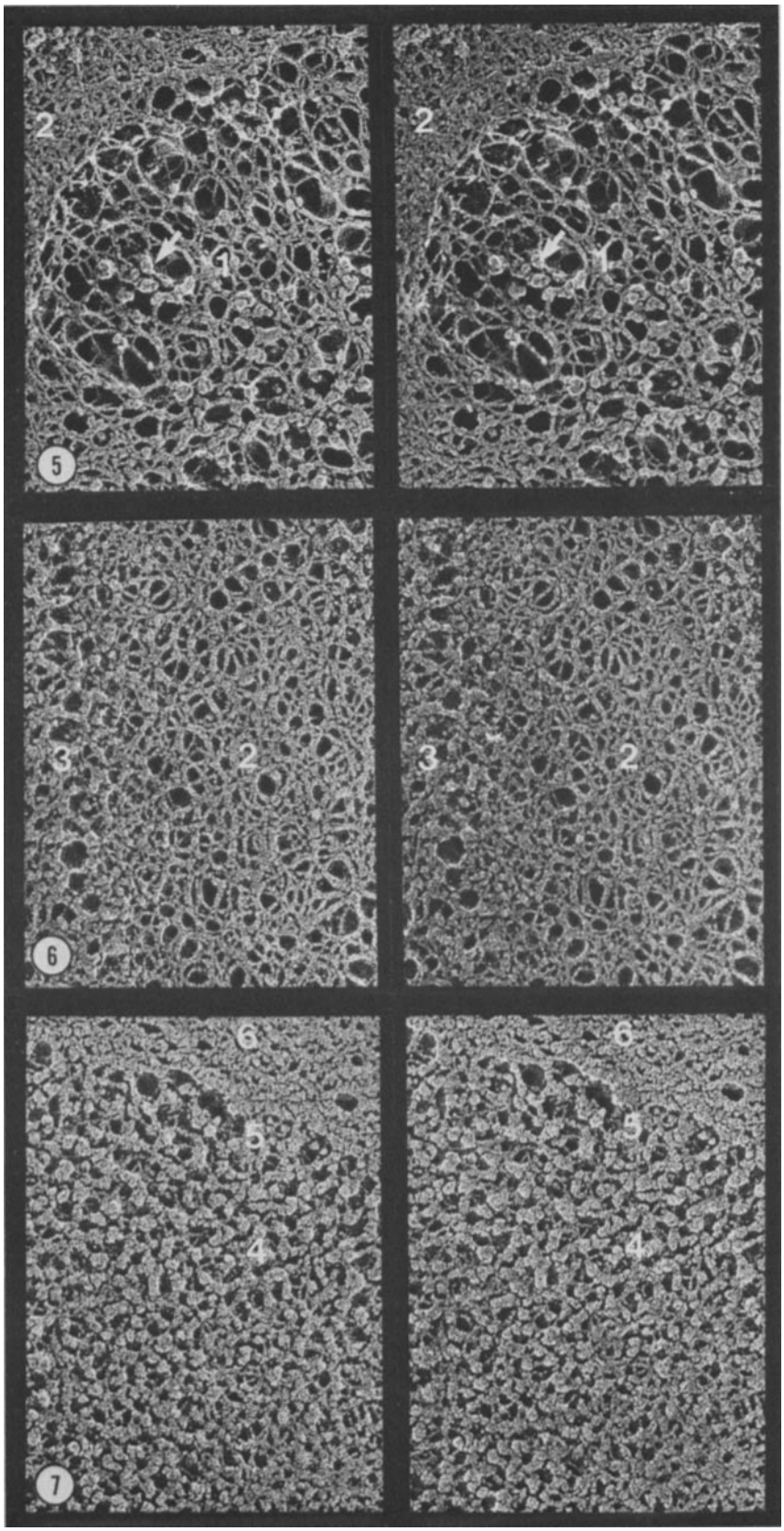

FIGURES 5–10 Stereo views of individual wall layers from intact cells. (Fig. 5) W1 layer (*1*) extending from the plasma membrane (at lower right in the uncropped field) upward to the dense W2 layer (*2*) at left and top. In W1, granules (arrow) are typically associated with the trabecular meshwork. × 120,000. (Fig. 6) W2 layer (*2*) extending upward to the W3 "space" (*3*) transected by delicate fibers. × 165,000. (Fig. 7) W4 layer (*4*) extending upward to the W5 "space" (*5*) which, in turn, contacts the dense W6 layer (*6*). × 165,000. (Fig. 8) W6 layer, torn diagonally at right center during sample preparation, with the granular W4 layer at

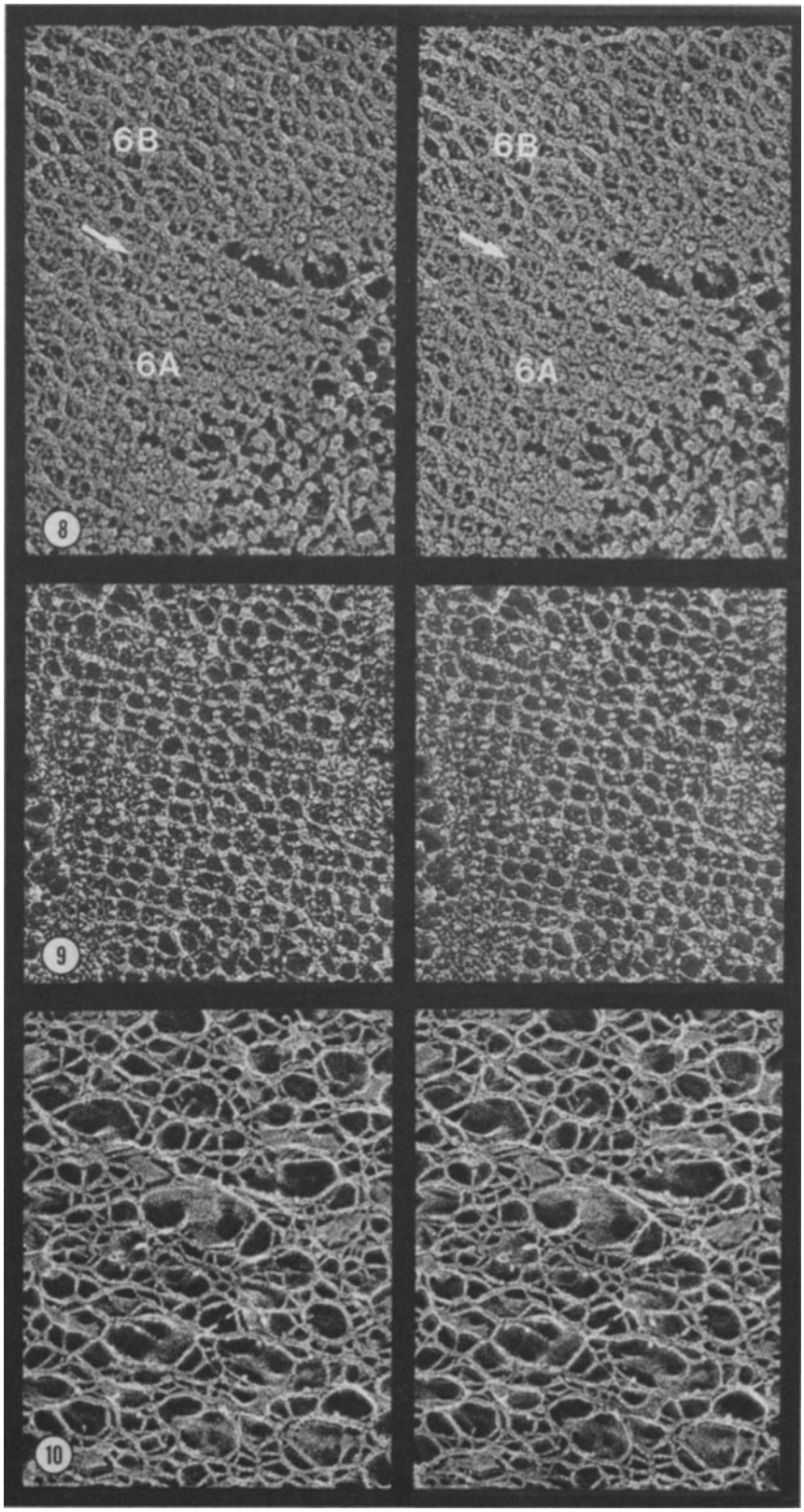

lower right. The layer is comprised of two sublayers. W6A is constructed from thick strands running parallel to the diagonal tear, which has occurred between two of the strands. These are interconnected by narrow fibrils, a cluster being marked by the arrow. W6B is constructed of an open weave of fibers, seen more clearly in Fig. 9. × 165,000 (Fig. 9) Polygonal weave constituting the W6B sublayer of W6. × 165,000. (Fig. 10) Outer W7 layer. × 120,000.

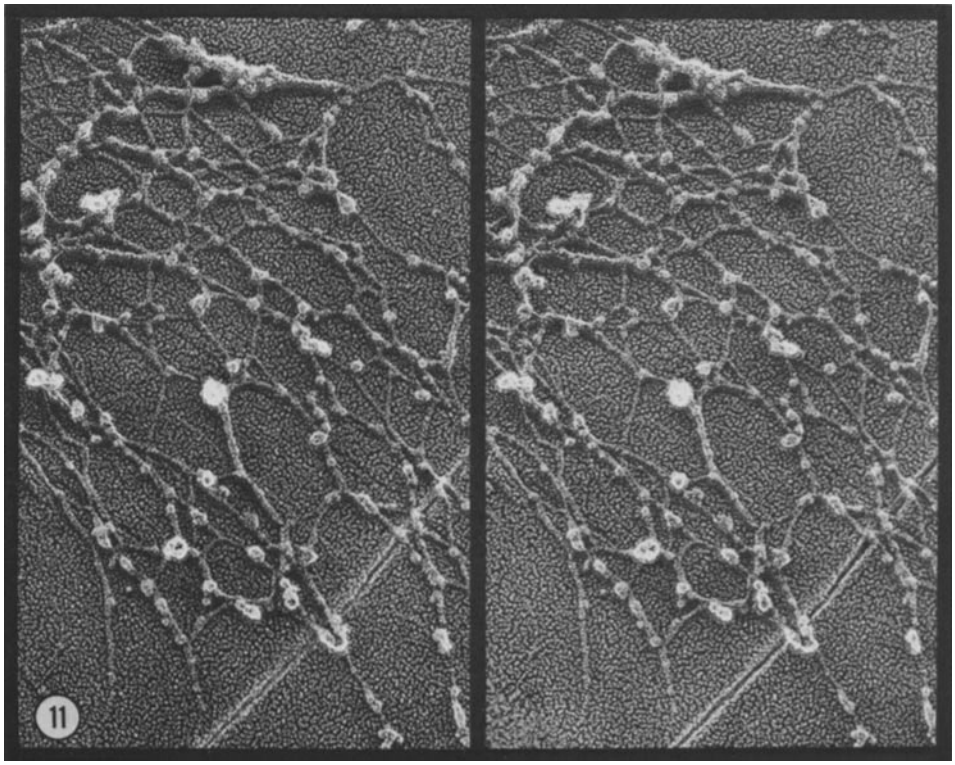

FIGURE 11 Stereoview of fibers of the W7 layer absorbed to mica (the uncropped micrograph includes an intact cell wall, only the peripheral W7 fibers of which made contact with the mica). × 120,000.

apparently devoid of all surface fibers (contrary to an earlier study from this laboratory [16] in which an incomplete removal was observed). However, after autolysin is washed away, the cell surface quickly acquires a coat of radial fibers (Fig. 12) similar to that seen in our earlier report (16). Discontinuous plaques of laminar material then appear within this trabeculum (Fig. 13, where discontinuities are indicated by arrows). These plaques enlarge in size until they contact to form a continuous layer (Fig. 14). *En face* views demonstrate that this primary lamina is organized like sublayer W6A (not shown). The medial and inner layers then assemble beneath this primitive W6 layer (Fig. 14, arrow).

We interpret these images to indicate that the W1 and W7 fibers are morphologically continuous with one another and constitute the original "warp" of the wall fabric. The elements of the central triplet are then assembled within this continuum to form the "weft." As the wall matures, the fibers in the W1 and W7 regions may well undergo distinctive chemical modifications and/or associate with distinctive materials (e.g., granules become localized exclusively in W1 [Figs. 3 and 5]). Therefore, W1 and W7 may have quite different biochemical and functional properties in the mature matrix (cf. reference 6).

Structure of the W6 Layer

When intact walls isolated from *bald-2* cells are sonicated or homogenized, the W6 layer frequently separates from its underlying layers and forms discrete fragments. Fig. 15 shows such a fragment that has adsorbed to mica by its undersurface (that is, the surface normally facing the cell membrane), where the W6A and W6B domains appear much as in replicas of the intact wall (Figs. 3, 4, 8–10). Fig. 16, by contrast, shows a fragment adsorbed by its upper surface, so that its undersurface is exposed to view. The undersurface, not normally visible in intact walls, displays a prominent lattice of globular units which define a series of parallelograms.

Fig. 17*A* diagrams the units of this W6 "undersurface" lattice as seen in deep-etch images, where the four major morphological units are designated *A–D*. Their crystalline spacing defines three major lattice planes, disposed as drawn in Fig. 17*B*. In Fig. 17*C* we have redrawn, to the same scale and orientation, an optical reconstruction of negatively stained W6 material obtained by P. Shaw and K. Roberts (15, 26). There is clearly excellent correspondence between the positions of the major foci deduced by the two techniques.

Fig. 17*D* diagrams the polygonal units that form sublayer W6B (Figs. 8 and 9). The foci of this array are superimposable on the major foci of the W6A crystal (Figs. 17, *A–C*), leading us to propose that the two arrays represent interacting sublayers of a single wall domain, W6.

In Vitro Assembly and Dissassembly of the W6 Crystal

Catt et al. (27) have demonstrated that when purified cell walls are solubilized in 1 M perchlorate and the extract is subjected to Sepharose 2B chromatography, a fraction designated 2BII is obtained which, when dialyzed against water, assembles into crystals with the same lattice parameters as the W6 layer in situ (27). SDS PAGE of the 2BII fraction reveals the presence of four glycopolypeptides (5). We have found that we can generate apparently identical crystals by a simpler procedure, namely, by extracting living *bald-2* cells with 1 M perchlorate, dialyzing and lyophilizing the extract, redissolving the lyophilate in 1 M perchlorate, and allowing this concentrated extract to dialyze (see Materials and Methods

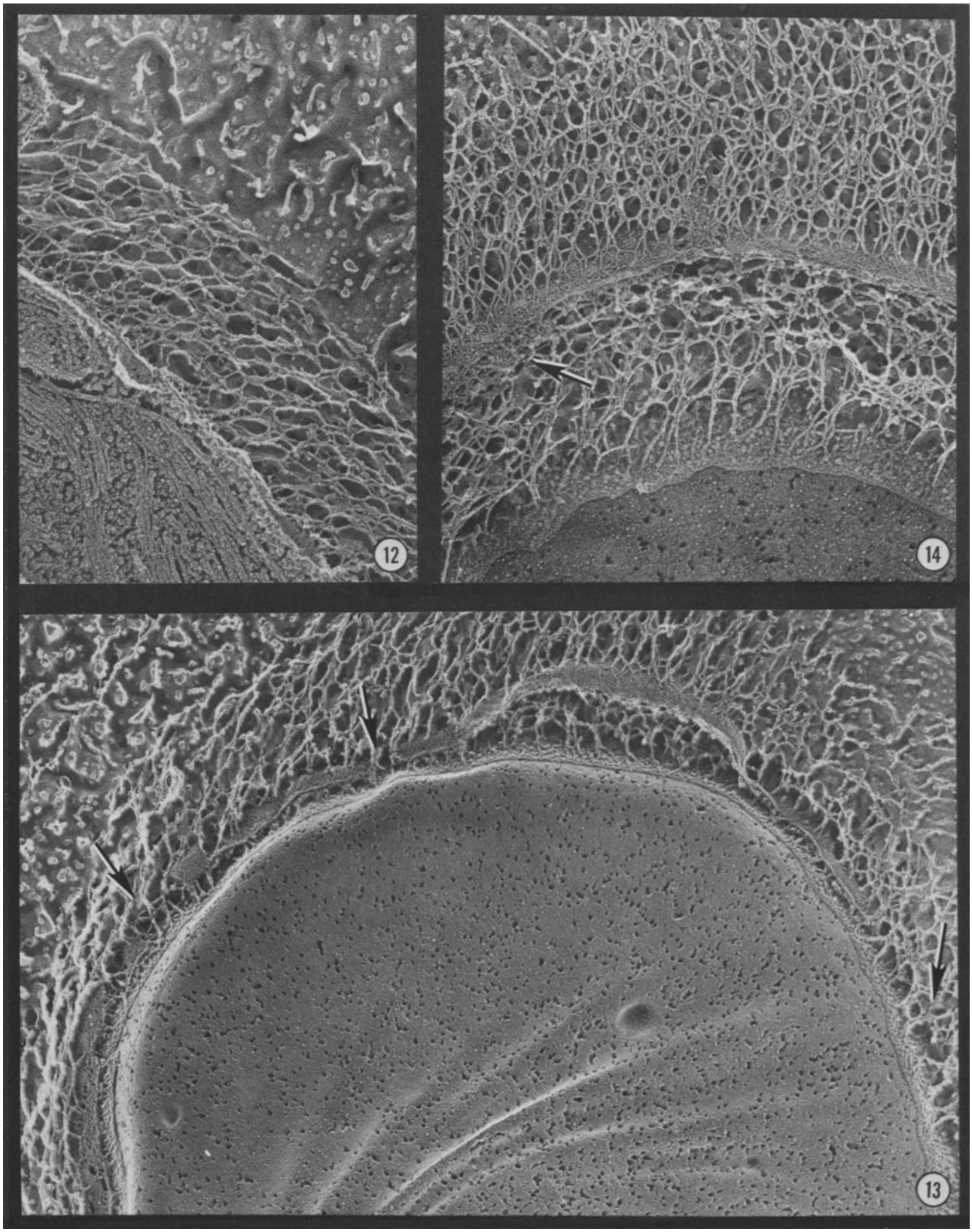

FIGURES 12–14 Regrowth of vegetative wall after autolysin treatment of intact vegetative cells. (Fig. 12) 1 h after stripping, showing new radial fibers. × 60,000. (Fig. 13) 2 h after stripping, showing discontinuities (arrows) in the assembling W6 layer. × 55,000. (Fig. 14) 3 h after stripping, showing new W6 layer and onset of W2 accumulation (arrow). Association of W1 fibers with the cell surface is seen to advantage. Note that the polygonal weave has not yet formed in the W6 layer. × 60,000

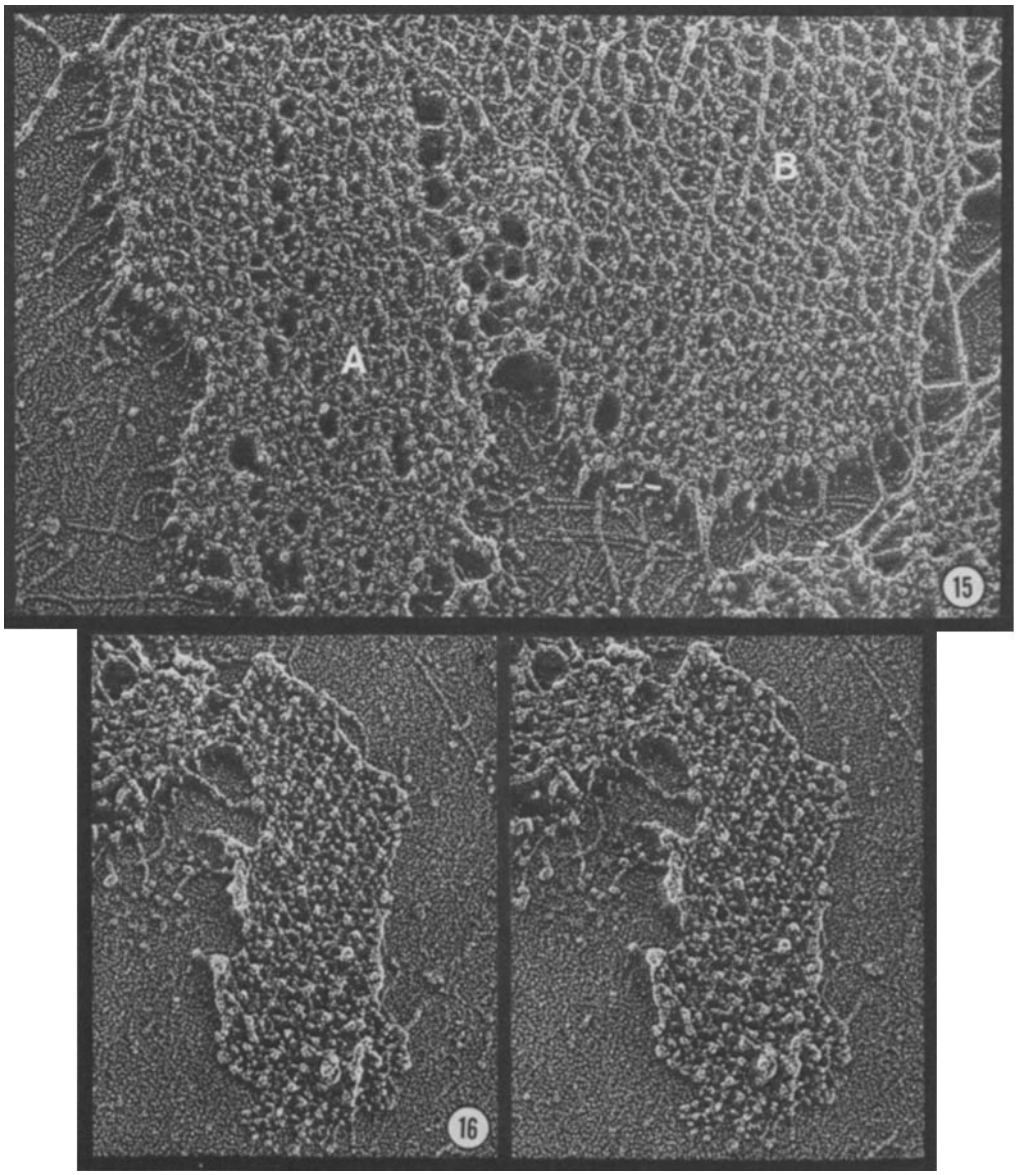

FIGURES 15 and 16 Fragments of the W6 layer. (Fig. 15) Upper surface of fragment recovered from a Virtis-homogenized preparation of isolated vegetative *bald-2* cell walls. *A*, W6A layer; *B*, W6B layer. × 170,000. (Fig. 16) Stereo pair of the undersurface of a W6 fragment from a sonicated *bald-2* cell wall preparation. × 165,000.

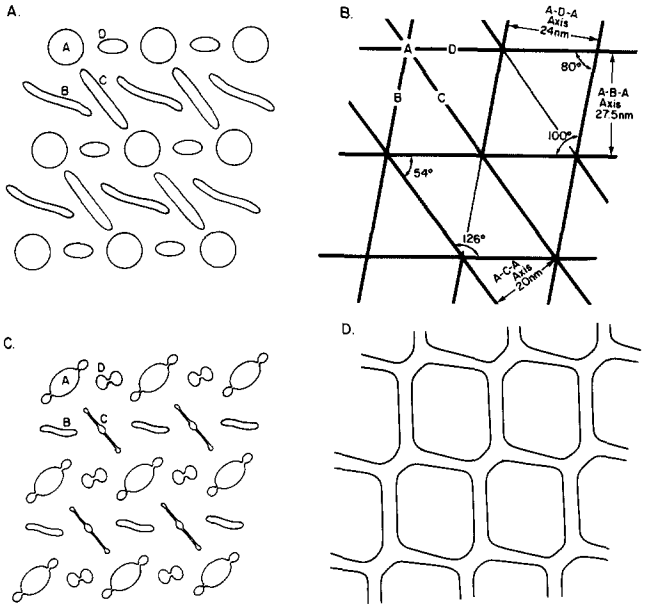

FIGURE 17 (*A*) Diagram of the undersurface of the W6 layer based on camera-lucida drawings of images such as Fig. 16. The fibrous elements *B* and/or *C* may represent "inside views" of the W6B system. (*B*) Lattice planes defined by the major foci (*A–D*) in Fig. 17*A*. A nearly upright parallelogram (80° by 100°) and a more obtuse parallelogram (54° by 126°) are evident. (*C*) Optical reconstruction of the W6 lattice from a negatively stained image, produced by Roberts et al. (15) and Roberts (26) and redrawn here with the same orientation and to the same scale as the other diagrams. (*D*). Diagram of the W6B polygonal network (Fig. 9) drawn to the same scale as *A–C*.

for details). At least 50 mg of pure crystals can in this way be prepared from a 5-liter culture. SDS PAGE of these crystals (Fig. 18) reveals the same four major glycopolypeptides that are present in 2BII fractions (5). Deep-etch replicas of the undersurfaces of both the 2BII crystals (Fig. 19) and the *bald-2* crystals (Fig. 20) show the same lattice organization found in native W6 fragments (Figs. 16 and 17).

Particularly instructive is the tendency of these crystals to disassemble as they absorb to mica, permitting views of their component glycoproteins. A detailed analysis of such images is underway; here we report two initial major findings.

First, it is clear from viewing the intact crystal that the W6A undersurface (Fig. 19) must be constructed from glycoproteins having discrete globular domains, corresponding to domains A and D in Fig. 17. In the periphery of disassembling crystals we find elongated globular elements—presumably glycoproteins—indicated by black arrowheads in Fig. 19 and, more clearly, in Fig. 20. They vary considerably in length, from ~50 to 70 nm depending on how distended they are on the mica. The caliber of their globular domains is sufficiently similar to those in the crystal to suggest that they interact to form the W6A sublayer (cf. Fig. 1*B*), but we have not yet deduced how these interactions take place.

It is also clear from viewing the intact crystal that its upper layer (W6B) must be constructed from glycoproteins that are predominantly fibrous, creating the open polygonal meshwork shown in Figs. 9, 15, and 17*D*. In Figure 19, the arrows

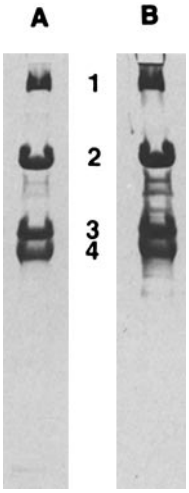

FIGURE 18 SDS PAGE of crystals harvested from a dialyzed *bald-2* perchlorate extract. The same gel was stained first by the periodic acid–Schiff procedure (*A*) and then by silver stain (*B*). The four major glycopolypeptides of the crystal (13) are labeled *1–4*. Three minor glycopolypeptides migrate between bands *2* and *3*. A few minor bands migrating below band *4* stain only with silver. Gel system and periodic acid–Schiff staining as in reference 16; silver staining was performed according to the procedure of Morrissey (44).

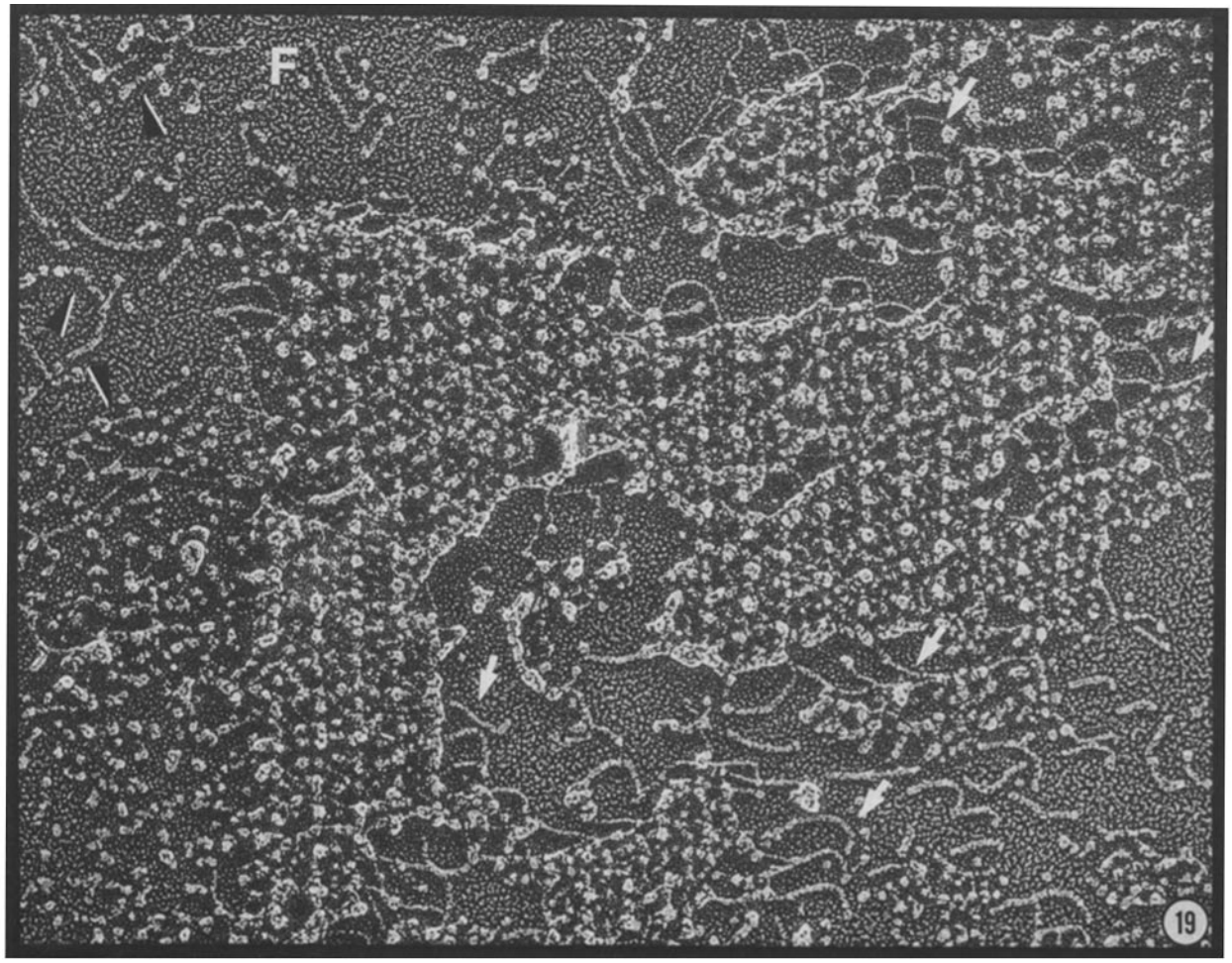

FIGURE 19 W6 material that has assembled in vitro after dialysis of a Sepharose 2BII fraction of a perchlorate extract, adsorbed to mica. The same crystalline lattice seen for the undersurface of homogenized wall fragments (Fig. 16) is present in the reassembled material. The crystal has undergone partial disassembly into globular (arrowheads) and fibrous (*F*) units. Arrows indicate regions where a fibrous meshwork is exposed. × 200,000.

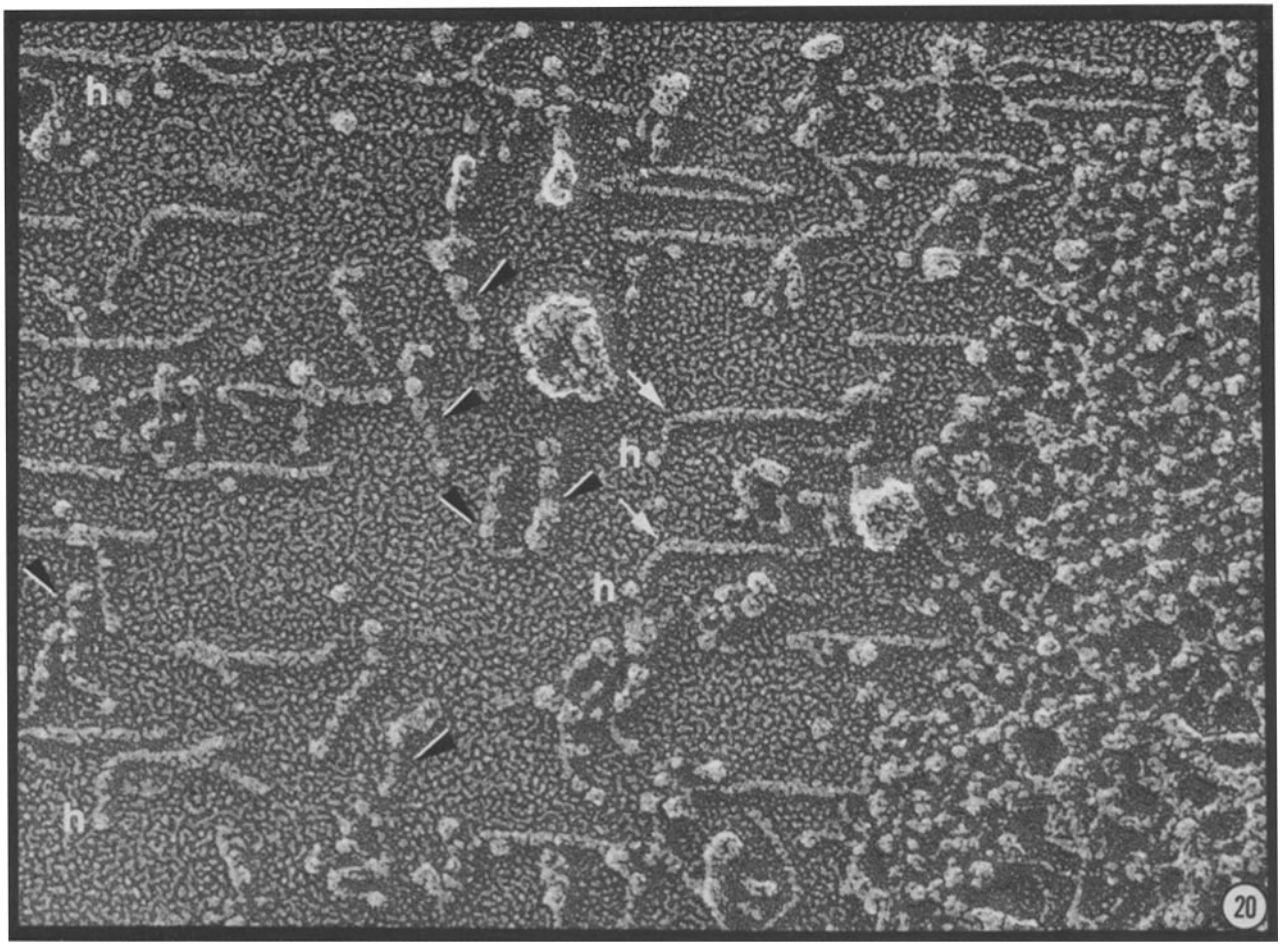

FIGURE 20 W6 crystal (*right*), polymerized in vitro from a *bald-2* extract, disassembling as it contacts the mica surface into two species of glycoprotein, one fibrous and one globular. The 100-nm fibers are aligned horizontally; each carries a head (*h*) at one end and may kink (arrows) along it shaft. Chains of globular domains (arrowheads), aligned vertically, resemble the globular components of the crystal. × 350,000.

denote regions where the globular glycoproteins are absent and an underlying system of fibers is exposed. The fibers are seen to interact with one another to form a network, leading us to propose that they constitute the polygonal meshwork. Individual fibers of this class are seen at F in Fig. 19 and are prominent in Fig. 20, where they align along the horizontal axis of the field (note that the globular glycoproteins [arrowheads] align along the vertical axis, suggesting that the two species respond to opposite properties of the mica crystal). Each fiber measures 102 ± 7 nm (n = 55) and carries a head at one end; some are straight, some are curved, and some make distinct kinks along their shaft (arrows). These glycoproteins are presumably equivalent to the 100-nm fibers visualized by Roberts (26) in 2BII fractions. We are currently seeking to understand how the fibers interact to form the W6B layer and how they align with components of the underlying W6A layer; we are also asking which of the four glycopolypeptides in the crystal (Fig. 18) forms which domains of the crystal glycoproteins.

The W2 Layer

When isolated cell walls are treated with 1 M perchlorate or other chaotropes, an insoluble, phase-transparent, wall-shaped residue remains which Hills et al. (14) interpreted to be W1. Repeating these experiments with isolated cell walls (Fig. 21) and with intact vegetative cells (Fig. 22), we conclude on the basis of morphology that the bulk of this insoluble material derives from the W2 layer, although a variable amount of the W1-W7 fiber system is also present.

FIGURES 21 and 22 Perchlorate-treated cell walls. (Fig. 21) Wall shed by the Norwich wild-type strain and treated with 1 M perchlorate. The residual layer corresponds to W2 in morphology. The flagellar collars (cf. reference 16), which are also insoluble in perchlorate (14), are labeled C. The W1/W7 system is absent, as is often the case for shed walls of the Norwich strain even before perchlorate extraction (data not shown). × 28,000. (Fig. 22) Vegetative *bald-2* cell incubated in 1 M perchlorate for 60 min. The W1, W2, and W7 layers, insoluble in perchlorate, continue to surround the cell, but the other wall layers have been removed. *CM*, cell membrane, *P* fracture face. × 56,000.

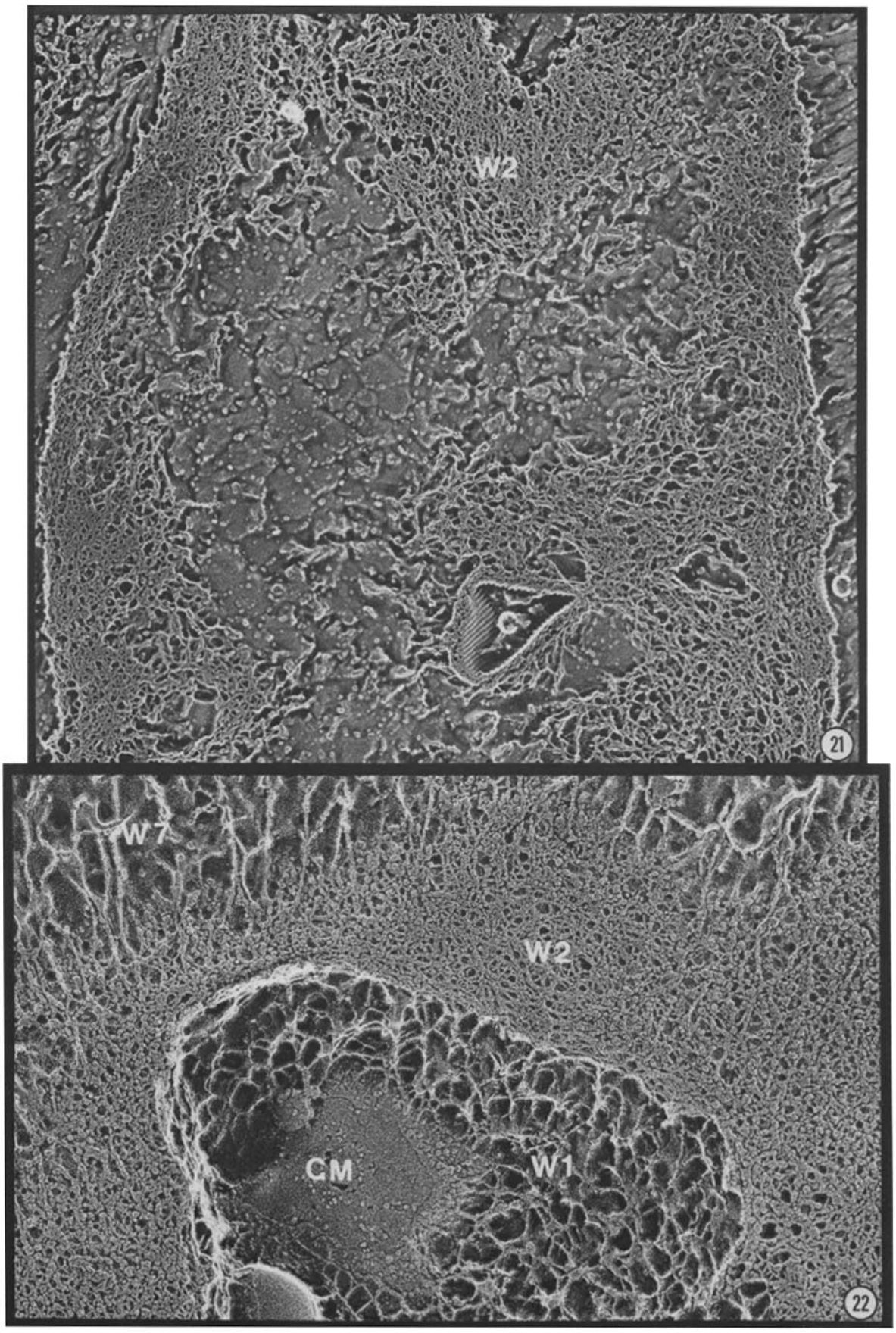
W2
C
C
21
W7
W2
CM
W1
22

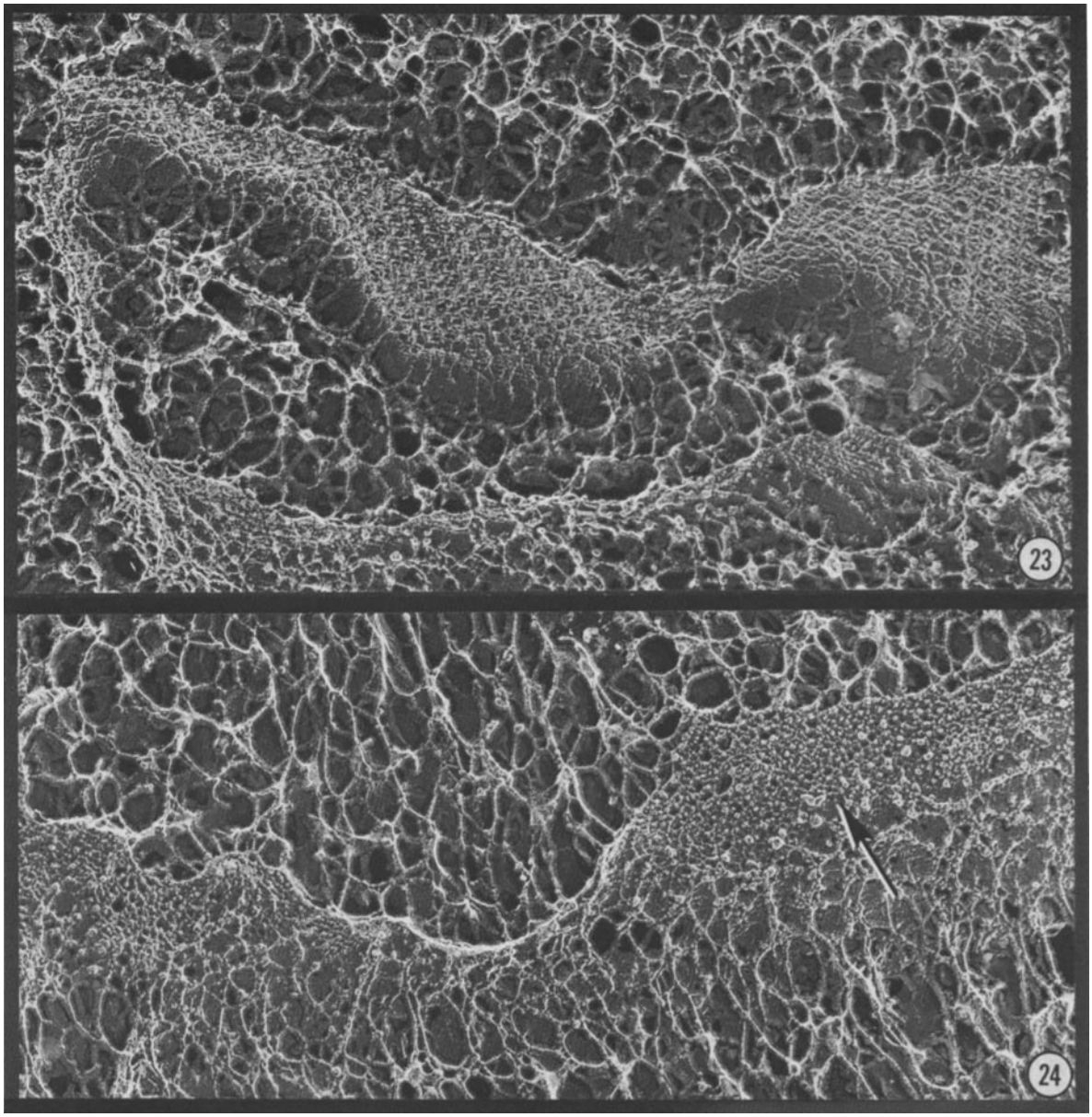

FIGURES 23 and 24 Cell walls shed during a *Chlamydomonas* mating and frozen after 20 min. (Fig. 23) The polygonal network of the W6B sublayer (cf. Fig. 9). (Fig. 24) The orthagonal crystalline lattice of the W6A undersurface (cf. Figs. 16 and 17). Fibrous trabeculae extend from both the upper and undersurfaces of the W6 layer, presumably deriving from the W1/W7 system. × 80,000.

Three experimental observations indicate that this W2 layer is disassembled by autolysin, the wall-disrupting agent released during the mating reaction between *Chlamydomonas* gametes. (*a*) If perchlorate-generated "ghosts" (Fig. 21) are exposed to autolysin, the ghosts dissolve. (*b*) Perchlorate-treated *bald-2* cells (Fig. 22) lose their surrounding W2 layer when exposed to autolysin. (*c*) Cell walls released into the medium during a normal mating reaction and frozen after 20 min display both the W6B (Fig. 23) and the W6A (Fig. 24) sublayers of W6 and retain trabeculae of W1 and W7 fibers; however, the W2 layer is absent. We conclude, therefore, that perchlorate and autolysin have reciprocal effects: perchlorate solubilizes W6 but not W2 (Figs. 21 and 22), whereas autolysin solubilizes W2 but fails, at least initially, to solubilize W6 (Figs. 23 and 24). Fragments such as those illustrated in Figures 23 and 24, we should note, are not stable: with time, they break up into smaller pieces and presumably disintegrate completely. Therefore, autolysin may have a slower-acting effect on W6. It is also important to note that when autolysin is secreted during the mating reaction, the cell wall is quickly released from the cell, much like an egg shell from an egg, its anterior end alone carrying a large tear (see reference 24). Therefore, the association between the W1 fibers and the plasma membrane must also be unstable to the presence of autolysin.

It follows from the above that the supernatant from a mixture of mating gametes should initially become filled with the products of W2 disintegration. Fig. 25 shows that such "mating supernatants" contain an abundance of fibrous units shaped like fishbones, with a central "spine" and "ribs" ra-

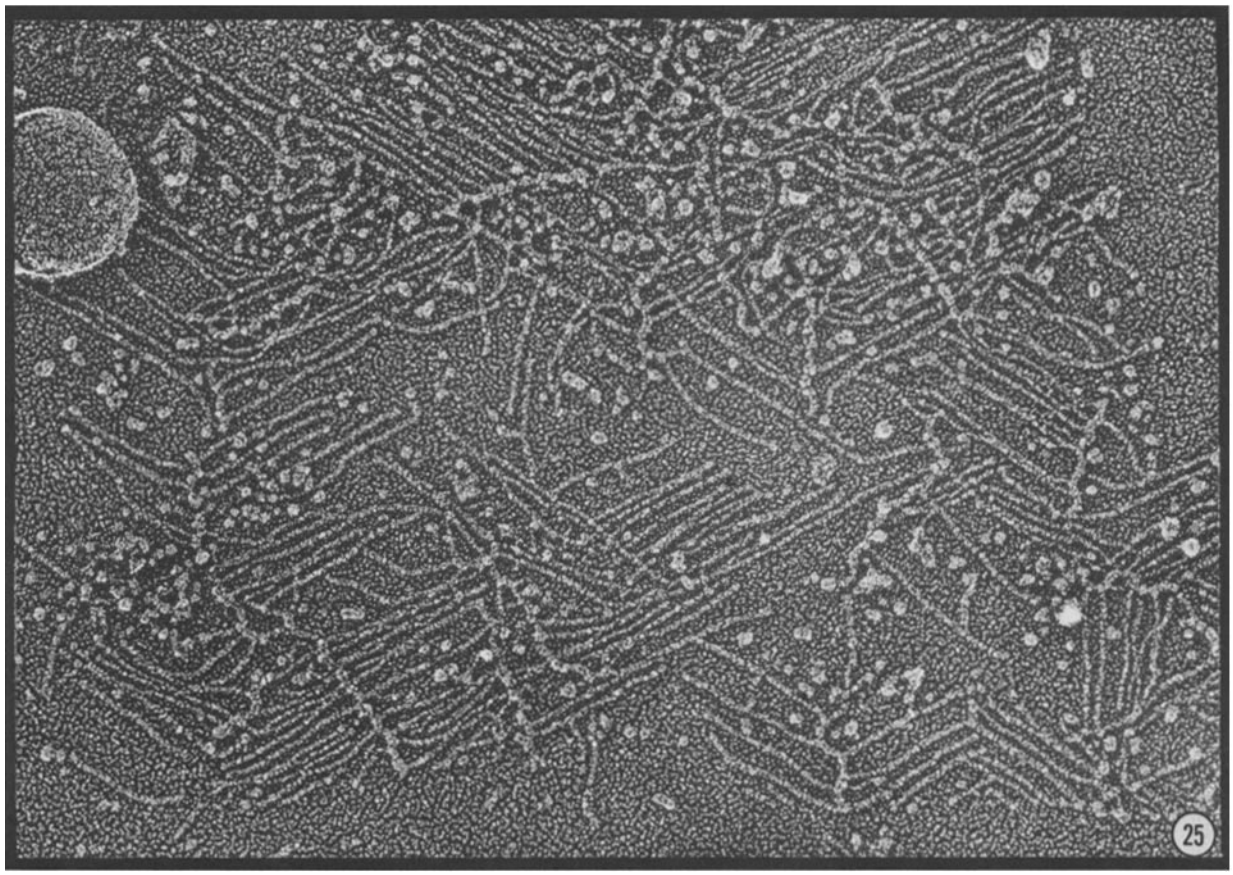

FIGURE 25 Mating supernatants adsorbed in mica. Fibrous components have the morphology of fishbones. Granular material is also present. × 217,000.

diating from either side. Fishbones are also released when perchlorate-treated wall "ghosts" (Fig. 21) are exposed to a partially purified preparation of autolysin (not shown). Thus we conclude that the W2 layer is constructed from fishbones, that these normally associate to form an insoluble matrix around the cell, and that the associations are sensitive to autolysin.

Figs. 26–29 illustrate features of fishbone construction. The central spine, when naked (Figs. 28 and 29, arrows), is a meandering unit, 127 ± 7 nm (n = 10) in length. When associated with ribs, the spine appears more acutely twisted (Figs. 26 and 27), suggesting that rib attachment causes it to deform, and it measures 137 ± 14 nm (n = 44) in length, the large standard deviation reflecting one's impression that some spines appear far more stretched out than others. There is considerable variability in the number of ribs attached per spine, but the maximum thus far encountered is 20, meaning that potential binding sites exist at least every 6 nm along the spine. The ribs are of two lengths: 195 ± 7 nm (n = 62) and 102 ± 8 nm (n = 152). It is perhaps significant that the long ribs are roughly twice the length of the short. Short ribs are more common than long, but no obvious pattern is followed in their attachment to the spine: some spines have no long ribs, some alternate long and short ribs, some have clusters of long ribs, and so on.

In situ, the W2 layer consists of stout and narrow fibers (Figs. 4, 6, 21, 22), suggesting that the spines may associate end-to-end to form the stout phase of the meshwork and that the ribs may reach out and bind to several spines to form the narrow interconnecting elements. We have not yet developed, however, a clear picture of how fishbones interact with one another.

Fig. 30 compares the SDS PAGE profile of intact cell walls (*A*) with perchlorate-insoluble wall residues (*B*). The major glycopolypeptides of the W6 layer (arrowheads) (see also Fig. 18) are depleted (but not absent) from the perchlorate-insoluble material (*B*) while other bands become more prominent. Imam et al. (29) recently reported that when isolated cell walls are treated with Sarkosyl-urea, they are converted to very thin walls that are degraded by autolysin. They report that these thin walls are not well solubilized for SDS PAGE in the normal SDS lysis buffer but only after boiling in lysis buffer containing concentrated (400 mM) dithiothreitol. Repeating their protocols, we find that three of the bands present in perchlorate-insoluble wall preparations (lane *B*) become far more prominent after boiling in dithiothreitol (lane *C*, arrows). The doublet band migrating at the 100 kD position in lane *C* may correspond to the polypeptide designated "mantelin" by Imam et al. (29). Taken together, it seems likely that the Sarkosyl-insoluble and perchlorate-insoluble wall layers are equivalent, and that both can be solubilized either by strong reducing conditions or by autolysin.

The Medial (W3-W5) Layer

If, as we proposed earlier, the W1/W7 fibers form the "warp" of the cell wall, then many of the slender fibers seen coursing through the medial layer (Figs. 2–4, 6, 7) can be presumed to derive from the W1/W7 system. In addition, the W4 layer contains a loose meshwork of associated granules,

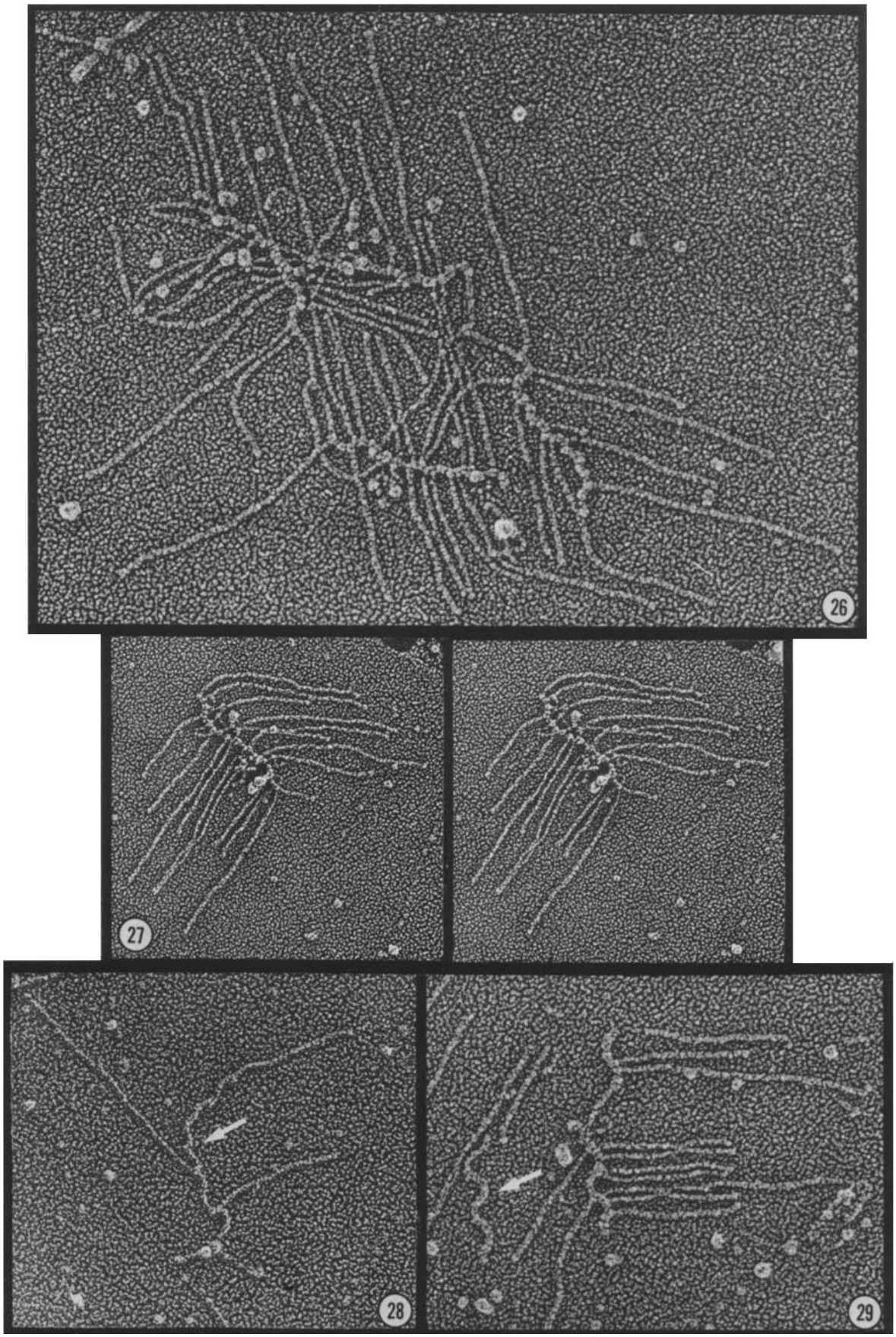

FIGURES 26–29 Fishbones. Fig. 27 is a stereo pair; Figs. 28 and 29 show disassembling units. Arrows, naked spines. (Fig. 26) × 280,000; (Fig. 27) × 165,000; (Figs. 28 and 29) × 280,000.

seen to advantage in Figs. 4 and 7. The granules are not visible in perchlorate-extracted walls (Figs. 21–22) nor in autolysin-generated outer layers (Figs. 23–24), but it is not known whether they are directly affected by perchlorate and autolysin or whether they simply "fall off" once the upper and lower layers separate.

Fibers Associated with the Flagellar Membrane

The flagellar membrane of *C. reinhardi* carries fibrous elements with sufficient structural homologies to the wall fibers to suggest that they are specified by a similar family of genes. Fig. 31 shows three sexual agglutinin "canes" and two "short canes," both species being displayed on the surface of gametic flagella (references 30–32). Included also in the plate are two fishbone ribs (Fig. 31) and a field of 100-nm fibrils from a Sepharose 2BII fraction (Fig. 32). Although dissimilar in length, the agglutinin cane and the 100-nm fibril are otherwise quite similar in morphology: both are equivalent in width, carry prominent heads, and display distinct kinks and bends along their shafts. The long and short ribs are similar in length to the long and short canes, respectively, but they are distinctly thinner, lack prominent heads, and never kink or bend. Collectively, therefore, the fishbones appear by morphology to be the more distantly related species.

Yet another element with structural homologies to the canes and the wall fibers is a woven array which we designate as a "hammock." A fully extended hammock is shown in Fig. 33, and a single "thread" of the net is shown in Fig. 34. Hammocks are encountered in purified flagellar preparations from both vegetative and gametic cells (reference 32); they are also encountered in mating supernatants, but not in cell wall preparations. They usually lie free on the mica, as in Figs. 33 and 34, but occasionally associate with the flagellar membrane in the fashion of a mastigoneme (references 33 and 34). Unlike the "ordinary" mastigonemes, however, which are composed of globular subunits (33), the hammocks have the distinctive fibrous structure described below.

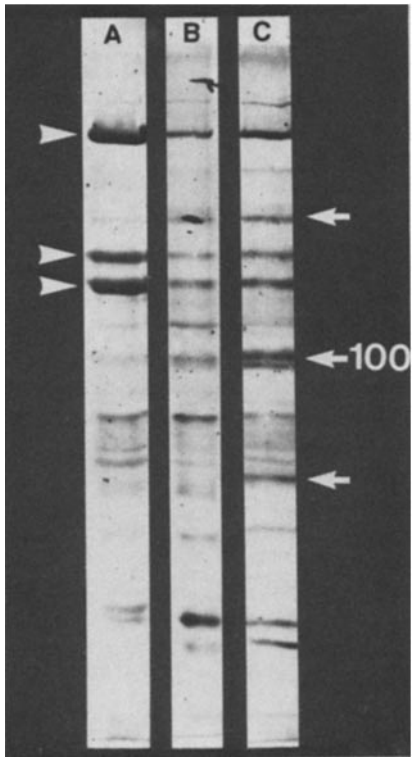

FIGURE 30 SDS PAGE of (*A*) intact walls, (*B*) perchlorate-insoluble wall material, and (*C*) the same sample as *B* but with 400 mM dithiothreitol in the lysis buffer (29). Three polypeptides (arrows), migrating as ~200-, 100-, and 70-kD species, are enriched in the high dithiothreitol sample. The 100-kD species may correspond to mantelin (29). Three of the four major glycopolypeptides of the W6 layer (Fig. 18) are indicated by arrowheads; the fourth, which migrates in the stacker (Fig. 18), is not included. Silver stain according to procedures outlined in reference 44.

The basic unit of the hammock is a check-shaped fibril, 55 ± 5 nm ($n = 18$) in length, with an invariant morphology: the first 80% of its length is a straight rod; it then makes a right-angle turn so that the final 20% is ~90° to the first. These fibrils interact in two planes: end-to-end and side-to-side. The end-to-end association creates long single threads (Fig. 34). A knob-like protuberance is present where the two ends join. Although we suspect that this represents a globular "head" like that on the 100-nm W6 fibril or the agglutinin, it may instead be created by the overlap of the fibrils; these alternatives cannot be distinguished until a means is found to dissociate the hammock into monomers. The side-to-side association, which is less stable to mica adsorption, involves an interaction between the knobs on one thread and the "right angles" on the adjacent thread. The right angles, we should note, are reminiscent of those formed by many of the dissociated 100-nm fibrils from the W6 layer (Figs. 19, 20, and 32), and the overall weave is reminiscent of the weave detected in the W6 crystals (Fig. 19) and in the W6B polygonal network (Fig. 9).

DISCUSSION

Chlamydomonas Wall Construction

Several levels of organization can be described for the cell wall of *Chlamydomonas*. The central domain is differentiated into three layers: an outer crystalline layer (W6), a medial granular layer (W4), and an inner dense layer (W2). Roberts and his collaborators have shown (5, 14, 27) that some of these layers can be solubilized by 1 M perchlorate and that they reassemble as the perchlorate is removed by dialysis; therefore, at least some of the layering must be established by hierarchies of protein–protein interactions and not, for example, solely by the sequential secretion of proteins during wall assembly. It follows that there must exist interactions between proteins in the same layer that hold it together, and also interactions between one layer and the next so that the whole assemblage holds together as a uniform 50-nm triplet.

A common mechanism used to ensure that elements in a given domain of the extracellular matrix remain together is to cross-link them after they co-assemble. Such cross-linking is used, for example, in the formation of elastin fibers (35), basal lamina (36, 37), and the primary wall of higher plants (37, 38). The W2 layer of the *Chlamydomonas* wall (Figs. 3, 4, and 6), if not covalently linked, is at least sufficiently bonded to resist dissociation by perchlorate or SDS (11), but is sensitive to the action of autolysin (present report). Imam et al. (29) have suggested that the wall possesses a "framework" held together by strong disulfide linkages and that autolysin dissociates these linkages. If, as we propose, the autolysin-sensitive framework is layer W2, and this layer is formed from fishbone units (Figs. 25–29), then disulfide linkages may hold ribs and/or spines together.

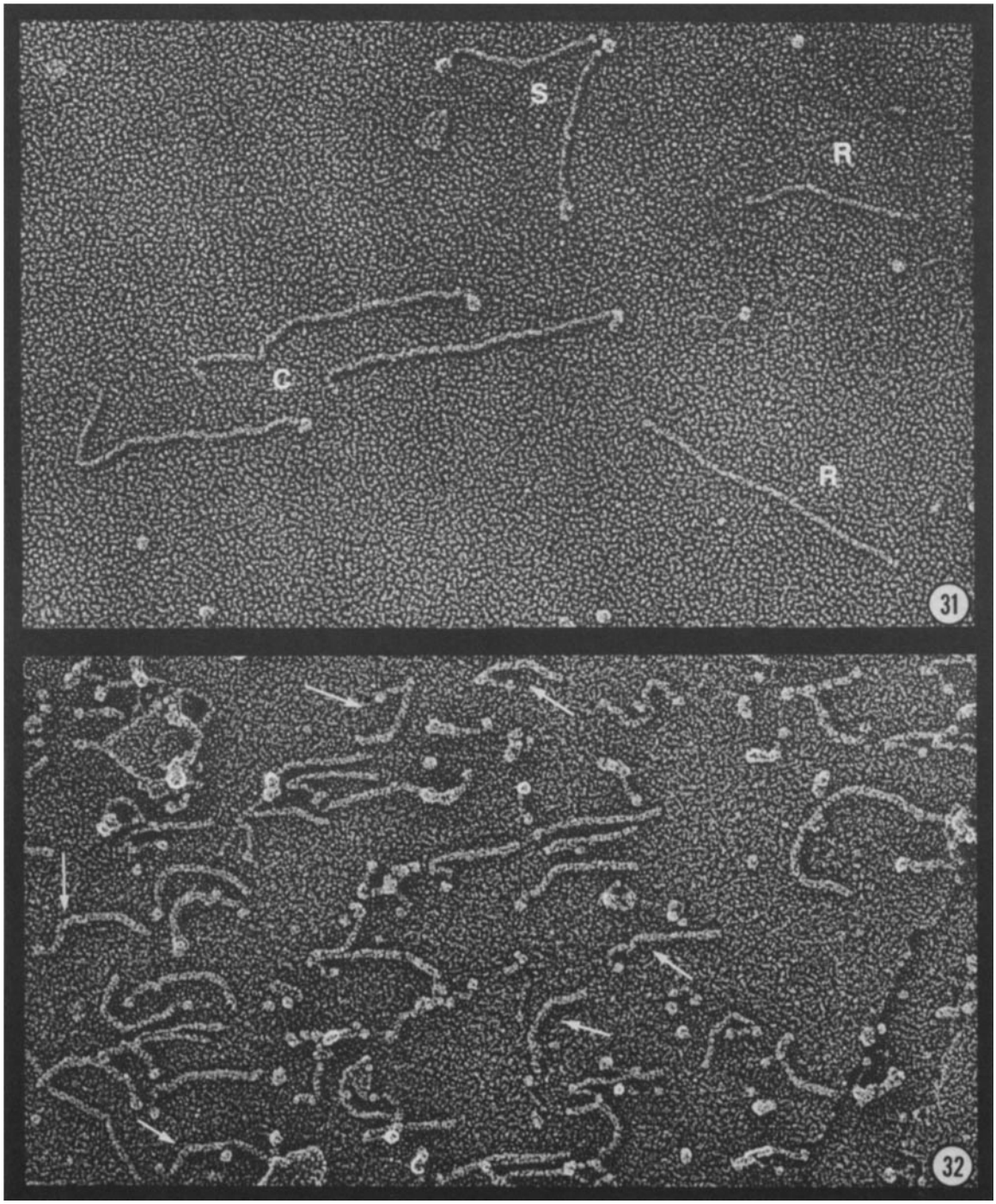

FIGURES 31 and 32 Purified flagellar surface and cell wall proteins. *C*, three sexual agglutinins, mt^+; *S*, two short canes associated by their termini; *R*, two ribs, one 100 nm and the other 200 nm, derived from fishbone units (Figs. 25–29). Fig. 32 shows 100-nm fibrils from the W6 layer purified by Sepharose chromatography; arrows designate examples of proteins that make kinks or bends in the fashion of agglutinin canes. Note that proteins with globular domains (cf. Fig. 20) are also present in this 2BII fraction. × 205,000.

The W6 and W4 layers, by contrast, are apparently not stabilized by covalent interactions, since they dissassemble in the presence of certain chaotropes (e.g., sodium perchlorate) or upon adsorption to mica surfaces. We predict, therefore, that these layers maintain their integrity via electrostatic and/or hydrophobic interactions amongst their constituent glycoproteins.

Studies of wall assembly, which are still in progress, define one of perhaps several systems which serve to integrate the various layers into a coherent unit. As shown in Figs. 12–14, radially disposed fibers initially extend from the cell membrane to the extremity of the W7 layer, and the three major layers of the central triplet then assemble within these fibers. Since the W6 layer can assemble in vitro in the absence of these fibers, they are clearly not essential for W6 polymerization. They may, however, contain a domain along their length which provides a nidus highly favorable to W6 polymerization, thereby assuring that the discontinuous W6 foci

(Fig. 13) merge to form a continuous layer. Certain *Chlamydomonas* mutants have been described that are unable to organize a wall around themselves but secrete wall proteins that polymerize normally in the medium (22); possibly some of these possess a defective W1/W7 system that fails to induce local W6 polymerization.

Fiber-to-Fiber Interactions in Chlamydomonas

In the animal basal lamina, the fibrous protein collagen IV has been shown to interact in both a head-to-head and a head-to-tail fashion to form extensive networks (39). We demonstrate here that much of the wall is formed of fibers that also interact to form networks. Whether by direct or parallel evolution, therefore, *Chlamydomonas* and animals appear to have come up with strikingly similar solutions to the construction of an extracellular matrix.

The hammock of *Chlamydomonas* (Figs. 33 and 34), although not a cell wall component per se, appears to be constructed from a wall-type of fibrous protein, and its mode of interaction can be directly visualized on the mica surface. The knobbed end of each hammock fiber proves to carry two binding sites, one with an affinity for the tail of another fiber, the other with an affinity for a bent domain along the shaft of another fiber. This bivalency permits both end-to-end and side-to-side interactions and hence the creation of a two-dimensional array.

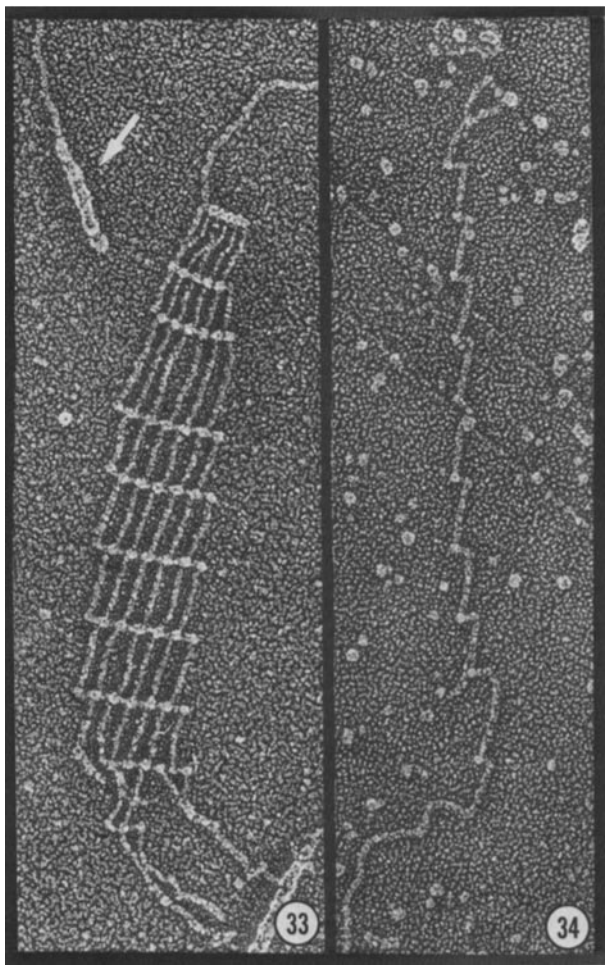

FIGURES 33 and 34 Hammock. Fig. 34 shows a single strand. Arrow, portion of a "regular" mastigoneme (33, 34). × 205,000.

When W6 crystals, polymerized in vitro, dissociate upon contact with mica, their upper surfaces are found to be composed of a fibrillar system wherein the fibers align in parallel rows and cross over to associate with fibers in adjacent rows (Fig. 19), highly reminiscent of the pattern found for the hammock array. The unit glycoprotein of this system appears to be a 100-nm fiber with a globular head (Figs. 20 and 32), and we propose that the system corresponds to the W6B network visualized in situ (Figs. 3, 9, and 17*D*).

Stafstrom and Staehelin (40) have recently reported that extensin, the major structural protein of higher plant cell walls, is an 81-nm fibrous protein that is "kinked" in several places. The presence of analogous kinks along the length of the 100-nm fibril (Figs. 20 and 32) suggests that such discontinuities may play an important role in wall construction throughout the plant kingdom.

The W2 layer is more complex than the hammock or W6B lattices in that it is composed of two distinctly different classes of fibrous proteins, spines and ribs. Moreover, the ribs are either 100 nm or 200 nm in length. Most importantly, the layer is clearly a three-dimensional network (Fig. 2), whereas the hammock and W6B are fundamentally two-dimensional. We imagine that the fishbone unit looks rather like a bottle brush in solution, with ribs radiating out in all directions, and that it contacts other such radiating units to create a three-dimensional array in situ.

In collaboration with Dr. David Kirk, we have used freeze-etching to examine the matrix surrounding the cells of *Volvox carteri*, whose cell wall is directly related to *C. reinhardi* (13). We find its W2 layer is indistinguishable from the *Chlamydomonas* equivalent. In *Volvox*, this W2 material increases greatly in thickness during expansion of the adult colony to accommodate the growing gonidia within the spheroid (41). The ability to create an expandable, three-dimensional W2 network would thus appear to have been critical to the evolution of the colonial mode in the Volvocales.

The final class of fibrous protein considered in this report is the sexual agglutinin of *Chlamydomonas*. We have previously shown this glycoprotein to be rich in hydroxyproline (31), and although the amino-acid composition of individual wall glycopolypeptides has not yet been determined, the glycoproteins as a whole are also rich in hydroxyproline (5, 14). Moreover, Adair (42) and Musgrave et al. (43) have found considerable antigenic cross-reactivity between the agglutinin and the wall glycoproteins, and the morphological similarities between the fibrous wall glycoproteins, the agglutinin, and the hammock units indicate that all probably belong to a similar biochemical family.

We are therefore led to propose the following evolutionary sequence. Fibrous hydroxyproline-rich glycoproteins were initially designed to self-assemble, after secretion, into an extracellular matrix designed to give structural support to the cell. Certain of these glycoproteins then came to be controlled by mating-type loci such that one version of an interacting dyad came to be displayed only on the surface of *plus* gametic flagella and the other on the surface of *minus* flagella, so that gametic recognition and adhesion become formally equivalent to cell wall assembly (31). At least some of the interactions between metazoan cells may follow a similar principle: cells destined to form a compound epithelium, for example, may display complementary collagen-like proteins which first recognize each other and then link the cells together by co-assembly.

We thank Dr. Keith Roberts for supplying his strain and for the reproduction used in Fig. 1, and Dr. William Snell for sharing his results on wall disassembly prior to publication. We also thank Robyn Roth for replicas, Lori van Houten for photography, Ann Dillon for the drawings, and Amy Papian for typing.

This work was supported by grants GM-26150 and GM-29647 from the National Institutes of Health.

Received for publication 19 December 1984, and in revised form 20 May 1985.

Note Added in Proof: Y. Matsuda et al. (*J. Biol. Chem.*, 1985, 260:6373–6377) have independently concluded that the perchlorate-insoluble portion of the *Chlamydomonas* wall is the target of autolysin activity.

REFERENCES

1. Trelstad, R. L., editor. 1984. Role of Extracellular Matrix in Development. New York, Alan R. Liss, Inc.
2. Lamport, D. T. A. 1980. Structure and function of glycoproteins. *In* The Biochemistry of Plants. J. Preiss, editor. Academic Press, Inc. New York. Vol. 3. 501–541.
3. Miller, D. H., D. T. A. Lamport, and M. Miller. 1972. Hydroxyproline heterooligosaccharides in *Chlamydomonas*. *Science (Wash. DC)*. 176:918–920.
4. Miller, D. H., J. S. Mellman, D. T. A. Lamport, and M. Miller. 1974. The chemical composition of the cell wall of *Chlamydomonas gymnogama* and the concept of a plant cell wall protein. *J. Cell Biol.* 63:420–429.
5. Catt, J. W., G. J. Hills, and K. Roberts. 1976. A structural protein, containing hydroxyproline, isolated from the cell wall of *Chlamydomonas reinhardi*. *Planta*. 131:165–171.
6. Fulton, A. B. 1978. Colonial development in *Pandorina morum*. I. Structure and composition of the extracellular matrix. *Dev. Biol.* 64:236–251.
7. Tautvydas, K. J. 1978. Isolation and characterization of an extracellular hydroxyproline-rich glycoprotein and a mannose-rich polysaccharide from *Eudorina californica* (Shaw). *Planta*. 140:213–220.
8. Lamport, D. T. A. 1974. The role of hydroxyproline-rich protein in the extracellular matrix of plants. *In* Macromolecules Regulating Growth and Development. E. D. Hay, T. J. King, and J. Papaconstantinou, editors. Academic Press, Inc. New York. 113–130.
9. Heuser, J. E. 1980. Three-dimensional visualization of coated vesicle formation in fibroblasts. *J. Cell Biol.* 84:560–583.
10. Heuser, J. E. 1983. Procedure for freeze-drying molecules adsorbed to mica flakes. *J. Mol. Biol.* 169:155–195.
11. Roberts, K., M. Gurney-Smith, and G. J. Hills. 1972. Structure, composition, and morphogenesis of the cell wall of *Chlamydomonas reinhardi*. I. Ultrastructure and preliminary chemical analysis. *J. Ultrastruct. Res.* 40:599–613.
12. Hills, G. J., M. Gurney-Smith, and K. Roberts. 1973. Structure, composition, and morphogenesis of the cell wall of *Chlamydomonas reinhardi*. II. Electron microscopy and optical diffraction analysis. *J. Ultrastruct. Res.* 43:179–192.
13. Roberts, K. 1974. Crystalline glycoprotein cell walls of algae: their structure, composition and assembly. *Philos. Trans. R. Soc. Lond. B Biol. Sci.* 268:129–146.
14. Hills, G. J., J. M. Phillips, M. R. Gay, and K. Roberts. 1975. Self-assembly of a plant cell wall *in vitro*. *J. Mol. Biol.* 96:431–441.
15. Roberts, K., G. J. Hills, and P. J. Shaw. 1982. The structure of algal cell walls. *In* Electron Microscopy of Proteins. J. R. Harris, editor. Academic Press Ltd. London. Vol. 3. 1–40.
16. Monk, B. C., W. S. Adair, R. A. Cohen, and U. W. Goodenough. 1983. Topography of *Chlamydomonas*: fine structure and polypeptide components of the gametic flagellar membrane surface and the cell wall. *Planta*. 158:517–533.
17. Kanwar, Y. S., and M. G. Farquhar. 1979. Anionic sites in the glomerular basement membrane. In vivo and in vitro localization to the laminae rarae by cationic probes. *J. Cell Biol.* 81:137–153.
18. Goodenough, U. W., and H. S. St. Clair. 1975. *Bald-2*: a mutation affecting the formation of doublet and triplet sets of microtubules in *Chlamydomonas reinhardi*. *J. Cell Biol.* 66:480–491.
19. Gorman, D. S., and R. P. Levine. 1965. Cytochrome f and plastocyanin: their sequence in the photosynthetic electron transport chain of *C. reinhardi*. *Proc. Natl. Acad. Sci. USA*. 54:1665–1669.
20. Martin, N. C., and U. W. Goodenough. 1975. Gametic differentiation in *Chlamydomonas reinhardtii*. I. Production of gametes and their fine structure. *J. Cell Biol.* 67:587–605.
21. Sueoka, N., K. S. Chiang, and J. G. Kates. 1967. Deoxyribonucleic acid replication in meiosis of *Chlamydomonas reinhardi*. I. Isotope transfer experiments with a strain producing eight zoospores. *J. Mol. Biol.* 25:47–66.
22. Davies, D. R., and A. Plaskitt. 1971. Genetical and structural analyses of cell-wall formation in *Chlamydomonas reinhardi*. *Genet. Res.* 17:33–43.
23. Snell, W. J. 1982. Study of the release of cell wall degrading enzymes during adhesion of *Chlamydomonas* gametes. *Exp. Cell Res.* 138:109–119.
24. Goodenough, U. W., and R. L. Weiss. 1975. Gametic differentiation in *Chlamydomonas reinhardi*. III. Cell wall lysis and microfilament-associated mating structure activation in wild-type and mutant strains. *J. Cell Biol.* 67:623–637.
25. Robinson, D. G., and U. G. Schlösser. 1978. Cell wall regeneration by protoplasts of *Chlamydomonas*. *Planta*. 141:83–92.
26. Roberts, K. 1981. Visualizing an insoluble glycoprotein. *Micron*. 12:185–186.
27. Catt, J. W., G. J. Hills, and K. Roberts. 1978. Cell wall glycoproteins from *Chlamydomonas reinhardii*, and their self-assembly. *Planta*. 138:91–98.
28. Claes, H. 1971. Autolyse der Zellwand bei den Gameten von *Chlamydomonas reinhardii*. *Arch. Mikrobiol.* 78:180–188.
29. Imam, S. H., H.-C. Shin, M. J. Buchanan, and W. J. Snell. 1984. Cell wall degradation in *Chlamydomonas*. *J. Cell Biol.* 99(4, Pt. 2):120a.
30. Adair, W. S., C. Hwang, and U. W. Goodenough. 1983. Identification and visualization of the sexual agglutinin from the mating-type plus flagellar membrane of *Chlamydomonas*. *Cell*. 33:183–193.
31. Cooper, J. B., W. S. Adair, R. P. Mecham, J. E. Heuser, and U. W. Goodenough. 1983. *Chlamydomonas* agglutinin is a hydroxyproline-rich glycoprotein. *Proc. Natl. Acad. Sci. USA*. 80:5898–5901.
32. Goodenough, U. W., W. S. Adair, P. Collin-Osdoby, and J. E. Heuser. 1985. Structure of *Chlamydomonas* agglutinin and related flagellar surface proteins in vitro and in situ. *J. Cell Biol.* 101:924–941.
33. Witman, G. B., K. Carlson, J. Berliner, and J. L. Rosenbaum. 1972. *Chlamydomonas* flagella. I. Isolation and electrophoretic analysis of microtubules, matrix, membranes, and mastigonemes. *J. Cell Biol.* 54:507–539.
34. Bergman, K., U. W. Goodenough, D. A. Goodenough, J. Jawitz, and H. Martin. 1975. Gametic differentiation in *Chlamydomonas reinhardtii*. II. Flagellar membranes and the agglutination reaction. *J. Cell Biol.* 67:606–622.
35. Franzblau, C., and B. Faris. 1981. Elastin. *In* Cell Biology of Extracellular Matrix. E. D. Hay, editor. Plenum Publishing Corp. New York. 65–93.
36. Linsenmayer, T. F., J.M. Fitch, and R. Mayne. 1984. Basement membrane structure and assembly: inferences from immunological studies with monoclonal antibodies. *In* The Role of Extracellular Matrix in Development. R. Trelstad, editor. Alan R. Liss, Inc. New York. 145–172.
37. Fry, S. C. 1981. Isodityrosine, a new cross-linking amino acid from plant cell-wall glycoprotein. *Biochem. J.* 204:449–455.
38. Cooper, J. B., and J. E. Varner. 1983. Insolubilization of the hydroxyproline-rich cell wall glycoprotein in aerated carrot root slices. *Biochem. Biophys. Res. Commun.* 112:161–167.
39. Timpl, R., H. Wiedemann, V. van Delden, H. Furthmayr, and K. Kuhn. 1981. A network model for the organization of type IV collagen molecules in basement membranes. *Eur. J. Biochem.* 120:203–211.
40. Stafstrom, J. P., and L. A. Staehelin. 1984. Structural studies on extensin, the major structural protein of plant cell walls. *J. Cell Biol.* 99(4, Pt. 2):244a.
41. McCracken, M. D., and W. J. Barcellona. 1983. Ultrastructure of sheath synthesis in *Volvox rousseletii*. *Cytobios*. 32:179–187.
42. Adair, W. S. 1985. Characterization of *Chlamydomonas* sexual agglutinins. *J. Cell Sci (Suppl. 1)*. In press.
43. Musgrave, A., P. de Wildt, R. Broekman, and H. van den Ende. 1983. The cell wall of *Chlamydomonas eugametos*. Immunological aspects. *Planta*. 158:82–89.
44. Morrissey, J. H. 1981. Silver stain for proteins in polyacrylamide gels: a modified procedure with enhanced uniform sensitivity. *Anal. Biochem.* 117:307–310.